4.

Near-Source Ground Motion and its Effects on Flexible Buildings

John F. Hall, M.EERI, Thomas H. Heaton, M.EERI, Marvin W. Halling, M.EERI, and David J. Wald, M.EERI

Occurrence of large earthquakes close to cities in California is inevitable. The resulting ground shaking will subject buildings in the near-source region to large, rapid displacement pulses which are not represented in design codes. The simulated M_w7.0 earthquake on a blind-thrust fault used in this study produces peak ground displacement and velocity of 200 cm and 180 cm/sec, respectively. Over an area of several hundred square kilometers in the near-source region, flexible frame and base-isolated buildings would experience severe nonlinear behavior including the possibility of collapse at some locations. The susceptibility of welded connections to fracture significantly increases the collapse potential of steel-frame buildings under strong ground motions of the type resulting from the M_w7.0 simulation. Because collapse of a building depends on many factors which are poorly understood, the results presented here regarding collapse should be interpreted carefully.

INTRODUCTION

Since the Northridge earthquake, there has been much discussion about the adequacy of building codes. Such an examination occurs after every damaging earthquake, and, in fact, the seismic provisions of building codes are based largely on experience from actual earthquakes. Because the Northridge earthquake occurred beneath a heavily urbanized area, it provided new information about the behavior of engineered structures located near a moderately large event. However, the region of largest long-period ground motions to the north of the epicenter is largely devoid of flexible buildings and so the Northridge earthquake did not fully test such structures. So there may well be some deficiencies in codes for Northridge-size earthquakes, and it is possible that there are more serious deficiencies for larger events

(JFH) Division of Engineering and Applied Science, Caltech, Pasadena, California 91125
(THH) Division of Engineering and Applied Science, Caltech, Pasadena, California 91125
MWH Department of Civil Engineering, Utah State University, Logan, Utah 84322
(DJW) U.S. Geological Survey, Pasadena, California 91104

©Earthquake Spectra, Volume 11, No. 4, November 1995

for which there is little experience. As earthquake magnitude increases, effects owing to duration, long-period ground motion and near-source pulses become more important, and in these respects current practice may be inadequate. For near-fault locations, the code section on base-isolated buildings requires site-specific analyses, which could produce satisfactory results if the ground-motion consultant makes a realistic recommendation. No such treatment for fixed-base buildings is required, even though some previous studies have shown that near-source ground pulses can make large demands on multistory structures (Bertero, et al., 1978; Anderson and Bertero, 1987).

The term "pulse" has been used with reference to acceleration, velocity and displacement descriptions of ground motion, i.e., an "acceleration pulse" or a "velocity pulse". Usage here will be for displacement pulse, defined as a ground displacement which is attained rapidly, say, with a peak velocity of 1 m/sec or greater. If the ground displacement itself is also large, say, a half meter or more, then the potential exists for causing considerable damage to flexible structures. A ground-displacement pulse is associated directly with the fault-rupture process, and although it may contribute significantly to the long-period content of the ground motion, it is distinct from other long-period motions such as arise from soft-soil effects or basin response.

It is no coincidence that the Northridge earthquake was the costliest in modern U.S. history, since it was also the largest earthquake to strike directly beneath a heavily urbanized area. Unfortunately, many of our urbanized areas will be struck by significantly larger earthquakes in the future. While peak accelerations in the near-source regions of these larger earthquakes are not expected to be much larger than those during the Northridge earthquake, ground-displacement pulses may be much larger.

This paper deals with structure response during a moderately large (M_W7.0) earthquake and focuses on near-source effects. Two background sections are presented first. One summarizes the potential for large earthquakes in some California urban areas with an emphasis on recent work in the greater Los Angeles metropolitan region. The other reviews current information about characteristics of near-source ground motion. For use in the engineering studies, a suite of ground motions from a simulated M_W7.0 blind-thrust earthquake is generated, as described in a separate section. Then, following a discussion of fundamental issues of how a tall building responds to near-source pulses, two detailed engineering studies are presented: one of a 20-story steel-frame building and one of a 3-story base-isolated building. Both buildings are examples of flexible structures which are vulnerable to near-source ground pulses. Since base-isolated buildings often house important functions such as medical treatment or emergency operations and, hence, are intended to remain functional after an earthquake, realistic treatment of ground motion is especially important. The Northridge earthquake revealed the susceptibility of steel buildings to weld fractures, and some preliminary analyses to assess the importance of this problem are also presented.

The engineering studies presented here deal with modern structures because there is uncertainty in how they will behave if subjected to strong near-source ground motions. It can be taken as fact that many types of older structures built before modern codes will fare poorly, and such structures are of the greatest concern.

POTENTIAL FOR LARGE EARTHQUAKES IN URBAN AREAS

Large earthquakes will occur in the future in the San Francisco Bay area which has already experienced a devastating M_w7.8 earthquake in 1906 on the San Andreas fault and also two earthquakes of about magnitude 7 in 1836 and 1868 on the Hayward fault. The 30-year probability of another San Francisco Bay area earthquake of M_w7.0 or larger has been estimated to be about 67% (Working Group on California Earthquake Probabilities, 1990).

Large earthquakes may be even more likely in Southern California. A recent study by the Southern California Earthquake Center (1994 Working Group on the Probabilities of Future Large Earthquakes in Southern California, 1995) concludes that the 30-year probability of a M_w7.0 or greater earthquake is 80 to 90 percent. While the San Andreas and San Jacinto faults are the most likely sources of such events, there are many other potential sources of large earthquakes in Southern California. In fact, the two biggest Southern California earthquakes of this century occurred on faults that were not recognized as likely candidates for very large events. The 1992 Landers earthquake (M_w7.3) ruptured along four distinct fault segments in the Mojave Desert (Sieh, et al., 1993). The occurrence of this earthquake casts doubt on the common assumption that the size of the largest earthquake to be expected in a region can be estimated from the length of the longest continuous fault segment. The M_w7.5 Kern County earthquake in 1952 was the greatest Southern California earthquake of this century. Despite its large size, only minimal surface rupture was identified for this mostly blind-thrust event (Buwalda and St. Armand, 1955).

Recent work by Dolan and others (1995) concludes that similar earthquakes are plausible beneath the greater Los Angeles metropolitan region where geodetic studies indicate a north-south shortening rate of about 8.5 mm per year. This shortening comes about as the region compresses into the bend in the San Andreas fault to the north. Six major fault systems (Figure 1) are of major concern because of their proximity to populated regions (Dolan, et al., 1995).

1. The Sierra Madre-Cucamonga thrust system borders the San Gabriel and San Fernando Valleys for 100 km along their northern edge. A 19-km segment of this system ruptured in the 1971 M_w6.7 Sylmar earthquake.

2. Underlying the most urbanized part of the region, the Los Angeles Basin fault system consists of the Elysian Park and Compton ramps, both major blind-thrust faults, and a flat connecting fault segment. Associated with this system are the Whittier and northern Newport-Inglewood faults which may be partitioned strike-slip faults above the blind-thrust faults.

3. The Santa Monica Mountain fault system extends 90 km westward from near downtown Los Angeles to along the Malibu coast. It contains a large blind-thrust ramp as well as the surficial Hollywood-Santa Monica-Malibu Coast strike-slip fault system.

4. The Oak Ridge thrust-fault system runs more than 70 km from Ventura eastward through the Santa Clarita River Valley, possibly including the previously unrecognized fault further to the east that generated the 1994 M_w6.7 Northridge earthquake.

5. The 40-km-long San Cayetano thrust fault lies along the northern edge of the Ventura Basin.

6. The Palos Verdes fault runs along the northeastern edge of the Palos Verdes Peninsula and extends offshore for more than 50 km to the south.

Dolan, et al. (1995) conclude that each of the six fault systems is capable of generating large earthquakes: M_w7.4 for the Sierra Madre-Cucamonga, M_w7.6 for the Los Angeles (or a M_w7.5 for the blind-thrust faults and a M_w7.1 for the Whittier fault, if they rupture separately), M_w7.5 for the Santa Monica (or a M_w7.2 for the blind-thrust component and a M_w7.3 for the Hollywood-Santa Monica-Malibu Coast strike-slip component, if they rupture separately), M_w7.3 for the Oak Ridge, M_w7.2 for the San Cayetano, and M_w7.2 for the Palos Verdes. However, it is more likely that each system breaks with a mix of earthquakes of various magnitudes.

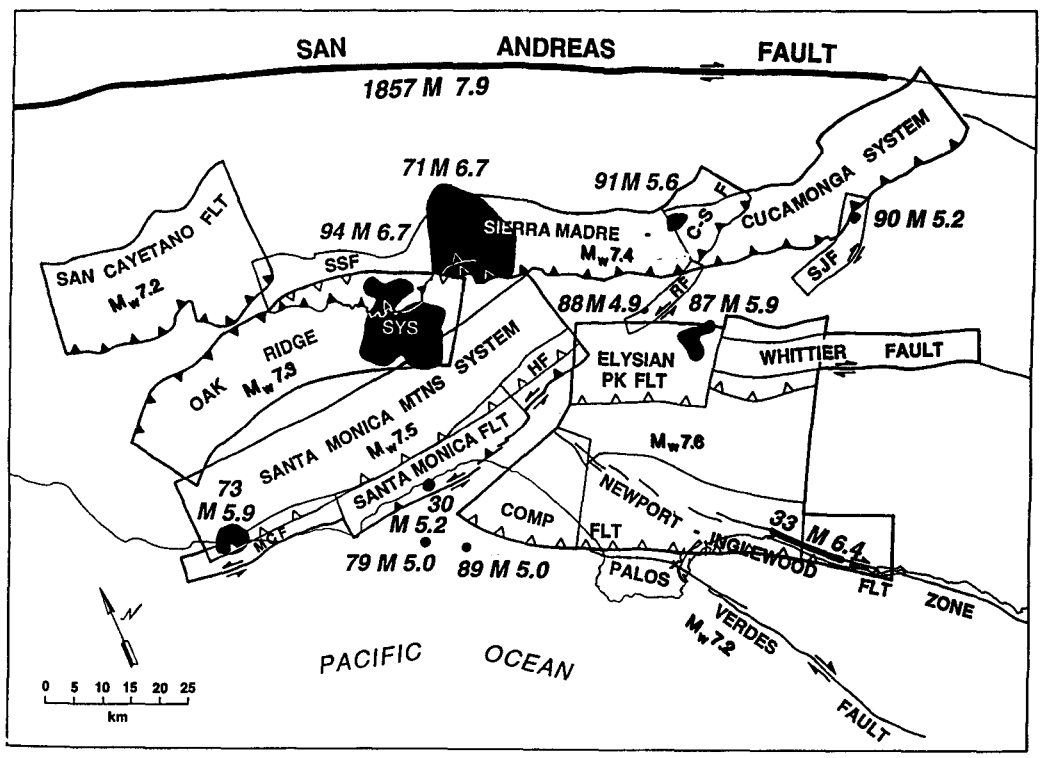

Figure 1 Map of the greater Los Angeles metropolitan region showing major fault systems capable of generating large earthquakes (Dolan, et al., 1995). Shaded regions and heavy lines indicate areas of historical fault rupture.

Dolan, et al. (1995) use estimates of geologic slip rates on these faults to conclude that the average interval between large earthquakes (M_w7.2 to 7.6) in the Los Angeles region may be as short as 140 years. Hough (1995) assumed a standard Gutenberg-Richter frequency-magnitude distribution and a convergence rate of 10 mm per year to calculate a recurrence interval of 203 years for M_w7.35 earthquakes. Hough's model yields an average interval of 90 years between events larger than M_w7.0.

The calculations of Dolan, et al. (1995) and Hough (1995) assume that slip only occurs in earthquakes; that is, fault creep is negligible. Recurrence intervals would be longer or magnitudes smaller if there is fault creep. Although there is no direct evidence that the thrust faults in the Los Angeles metropolitan region are creeping, such as the presence of microseismicity which appears to accompany deep creep on the San Andreas fault in central California, the possibility of creep is still an open issue (1994 Working Group on the Probabilities of Future Large Earthquakes in Southern California, 1995). However, the occurrence of M_w6.7 thrust earthquakes in 1971 and 1994 in the San Fernando Valley and the occurrence of the M_w7.5 Kern County earthquake in a similar tectonic environment implies that the M_w7.0 blind-thrust earthquake considered in detail later is a plausible event for the Los Angeles region.

NEAR-SOURCE GROUND MOTIONS

Several major urban areas in California are located alongside major active faults and so could be subjected to near-source ground motions from large earthquakes. The San Andreas fault runs 10 km west of downtown San Francisco and then extends southward through the peninsula near Daly City and other communities. Much of Oakland and other East Bay cities is within 10 km of the Hayward fault, and practically all of San Bernardino is within 10 km of either the San Andreas or San Jacinto faults. A large part of the greater Los Angeles metropolitan region lies atop buried thrust faults capable of generating earthquakes in excess of M_w7.0, as Figure 1 makes clear.

Knowledge of ground motion in the near-source region of large earthquakes is limited by the sparcity of recorded data. Table 1 lists peak ground accelerations, velocities and displacements from 30 known records obtained within 5 km of the surface projection of the rupture surface for M_w6.5 and greater earthquakes (Heaton, et al., 1995). The median peak ground acceleration and velocity from this table are 0.81g and 103 cm/sec, respectively; both are high values. Peak velocity is often viewed as a better indicator of damage potential than is peak acceleration, and velocity histories of several of the records listed in the table are shown in Figure 2. The large "velocity pulses" evident in the plots would be viewed as damaging by engineers, but the damage potential also depends on how much ground displacement occurs during these velocity pulses.

TABLE 1

Peak near-source ground motions from large earthquakes.

Earthquake	Distance* (km)	Acceleration (g)	Velocity (cm/s)	Displacement (cm)
1971 San Fernando, USA, M_w6.7				
Pacoima Dam	0	1.12	113	38
1978 Tabas, Iran, M_w7.4				
Tabas	3	0.92	125	106
1979 Imperial Valley, USA, M_w6.5				
El Centro Array 7	1	0.65	110	41
El Centro Array 6	1	1.74	110	55
Bonds Corner	4	0.81	44	15
El Centro Array 5	4	0.56	87	52
El Centro Array 8	4	0.64	53	29
1985 Nahanni, Canada, M_w6.8				
Site 1	0	>2.0	39	36
Site 2	0	0.50	31	31
1987 Superstition, USA, M_w6.6				
Parachute Test site	0	0.53	138	60
Superstition Mountain	6	0.91	44	15
1989 Loma Prieta, USA, M_w6.9				
Los Gatos Presentation Center	0	0.62	102	40
Lexington Dam	5	0.44	120	32
1992 Erzincan, Turkey, M_w6.8				
Erzincan	2	0.50	105	40
1992 Petrolia, USA, M_w7.0				
Cape Mendocino	0	>1.8	126	67
Petrolia	5	0.69	90	31
1993 Landers, USA, M_w7.2				
Lucerne	1	0.90	142	255
1994 Northridge, USA, M_w6.7				
Rinaldi Receiving Station	0	0.85	177	50
Sylmar Converter Station	0	0.90	129	50
Los Angeles Dam	0	0.32	79	22
Sepulveda Veterans Hospital	0	0.94	75	15
Jensen Filtration Plant	0	0.85	103	38
Sylmar County Hospital	2	0.91	134	44
Van Nuys (hotel)	2	0.47	48	13
Arleta fire station	4	0.59	44	15
Newhall fire station	5	0.63	101	36
Tarzana nursery	5	1.82		
1995 Hanshin, Japan, M_w6.9				
Kobe (JMA)	0	0.85	105	26

Earthquake	Distance* (km)	Acceleration (g)	Velocity (cm/s)	Displacement (cm)
Kobe University	0	0.31	55	18
Takatori	0		176	

*Approximate horizontal distance from the recording site to the surface projection of the rupture.

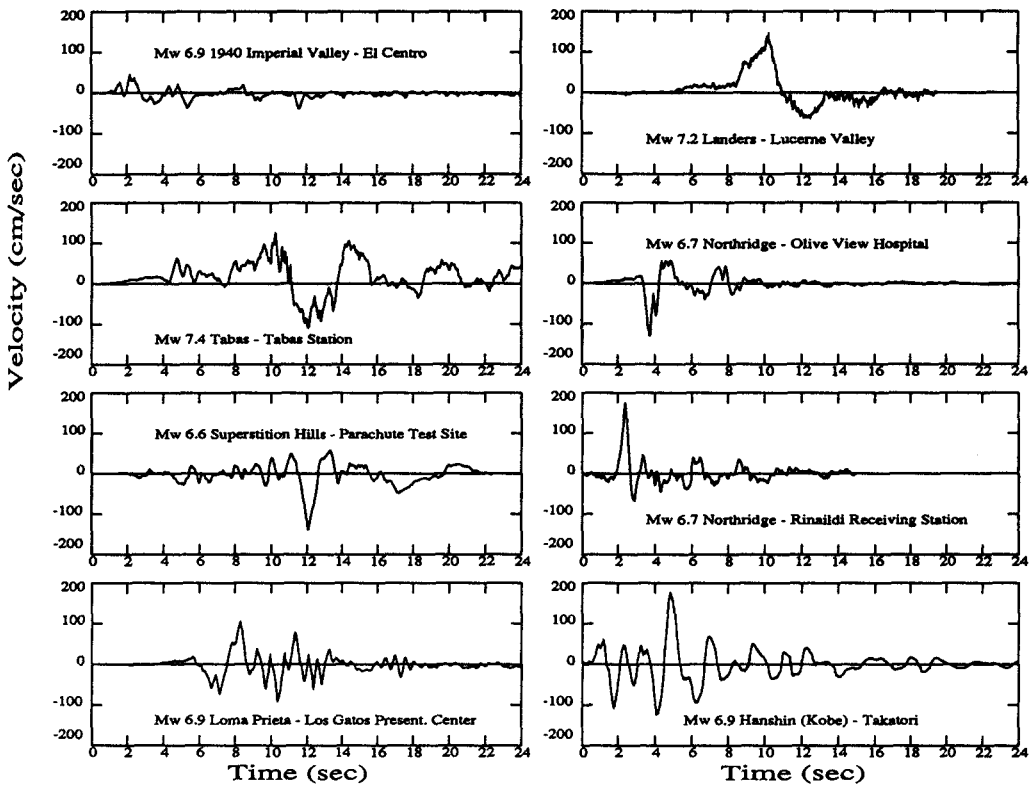

Figure 2 Sample of ground-velocity time histories from Table 1 containing high peak velocities.

The peak ground displacements in Table 1 are probably not accurate (too small) because the standard processing procedures remove part of the displacement through filtering. The 255-cm ground displacement in the Lucerne Valley record from the Landers earthquake is an exception as special processing was employed to preserve the displacements (Iwan and Chen, 1994). It should also be mentioned that the location of this instrument was near the end of the fault segment that ruptured, and so the 255-cm displacement should have been exceeded elsewhere. The ground velocity accompanying the 255-cm displacement measured at Lucerne Valley is 142 cm/sec. Wald and Heaton (1994a), using the same procedure as

described later, successfully modeled the long-period part of this record (>1 sec) and inferred that even higher velocities occurred at sites located further south along the rupture.

It is well known that significant ground displacements can accompany large earthquakes. The amplitude of the total slip (from one side to the other) along the surface trace of the fault reached 6 meters for the M_w7.3 Landers earthquake and 7 meters for the M_w7.8 San Francisco earthquake. This part of the ground displacement is referred to as the static component to distinguish it from that associated with seismic waves which are generated at the fault during rupture. This latter part of the ground displacement can also attain large amplitude in the near-source region because the shear wave which travels ahead of the fault-rupture front builds up owing to the shear-wave speed being only slightly higher than the speed of fault rupture (Archuleta and Hartzell, 1981). Displacement associated with this shear wave is largest in the direction perpendicular to the fault, and it can have similar amplitude to the static displacement parallel to the fault. Large displacements would be of little consequence if they occurred slowly (unless a structure straddled the fault). However, the duration of these displacements is closely related to the characteristic slip time of a point on the fault, and there is compelling evidence that this slip is rapid (Heaton, 1990). Thus, both the static and shear-wave displacements can occur as pulses. Further, a shear-wave displacement pulse can have both a forward and back phase (reversing pulse) which can be more damaging to a structure than the forward-only static pulse.

Existence of the shear-wave displacement pulse has not been fully appreciated for strike-slip faults (motion perpendicular to the fault), and it is also the reason why a blind-thrust earthquake can produce a large displacement pulse on the ground surface. The shear wave generated from an upward-traveling rupture on a dipping blind-thrust fault bends as it encounters lower velocity layers toward the surface, and the predominant motion tends to the horizontal.

Distribution of the shear-wave displacement pulse over the ground surface is very directional, as is evident by the pulse's origin. In general, the largest such pulses will strike sites located in the direction of the rupture. The famous record from the 1940 M_w6.9 El Centro earthquake, recorded in El Centro at a distance of 8 km from the fault rupture and which has commonly been taken as an example of near-source ground motion from a large strike-slip earthquake, has a peak ground velocity of only 43 cm/sec (Figure 2). Although little is known of the rupture history of this earthquake, an epicenter near El Centro is likely (Richter, 1958). If this is true, the shear-wave displacement pulse would have been directed away from the recording site. Similarly, the epicenter of the 1906 San Francisco earthquake was near the city (Bolt, 1968). Even for the Northridge earthquake, the recorded motions show that the highest velocities were directed off to the north into the northern part of the San Fernando Valley and into the Santa Susanna Mountains (an area largely devoid of flexible buildings) by the fault rupture proceeding up this south dipping fault (Figure 3) (Wald and Heaton, 1994b). On the other hand, for the recent M_w6.9 Hanshin (Kobe) earthquake, the city of Kobe lay along the strike-slip fault about 10 km northeast of the epicenter and so may have been hit by the shear-wave pulse. However, the effect could have been moderated by the bilateral rupture of this earthquake.

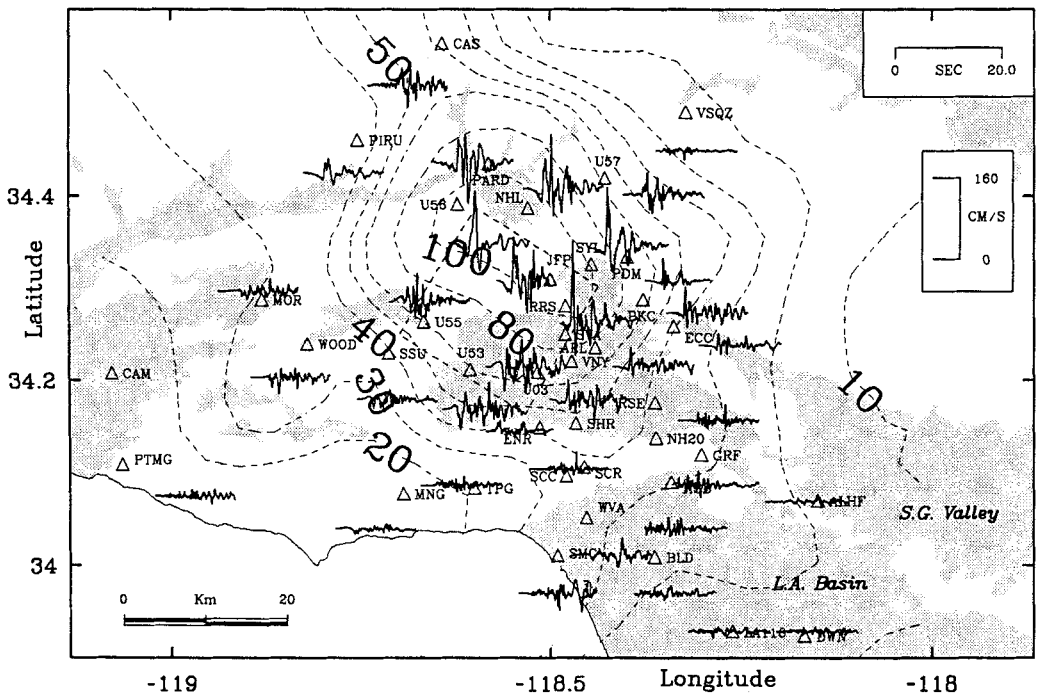

Figure 3 Sample of ground velocity time histories recorded during the Northridge earthquake, shown with peak velocity contours in cm/sec (Wald and Heaton, 1994b). Epicenter is marked by a star, and the dotted rectangle is the surface projection of the fault.

Because of the paucity of records from the near-source region of large earthquakes, reliance must be placed on simulations by seismologists in order to quantify the displacement-pulse effect. Near-source ground motions at periods of 1 second and greater have been successfully modelled for at least ten California earthquakes: 1971 San Fernando, 1979 Imperial Valley, 1984 Morgan Hill, 1986 North Palm Springs, 1987 Whittier Narrows, 1987 Superstition Hills, 1989 Loma Prieta, 1991 Sierra Madre, 1992 Landers and 1994 Northridge. References for these studies are listed by Heaton, et al. (1995). Although they were performed after the fact, seismologists believe that predictions can now be reliably made. Figure 4 shows a ground motion simulation made in 1990 for a M_w7.6 strike-slip earthquake (Hartzell and Heaton, 1990). The displacements parallel and perpendicular to the fault are the static and shear-wave displacement pulses, respectively. Although the rapid nature of such large displacements would have been viewed with skepticism by some engineers in 1990, they now seem quite possible considering the records from the M_w7.3 Landers earthquake at Lucerne Valley discussed above. The average slip on the fault was 5 meters for the simulated M_w7.6 earthquake and was about 3 meters (Wald and Heaton, 1994a) for the Landers earthquake. While a 5-meter average slip is infrequent, that on the 300-km-long north-coast segment of the San Andreas fault in 1906 averaged 7 meters in the crust (Working Group on California Earthquake Probabilities, 1988).

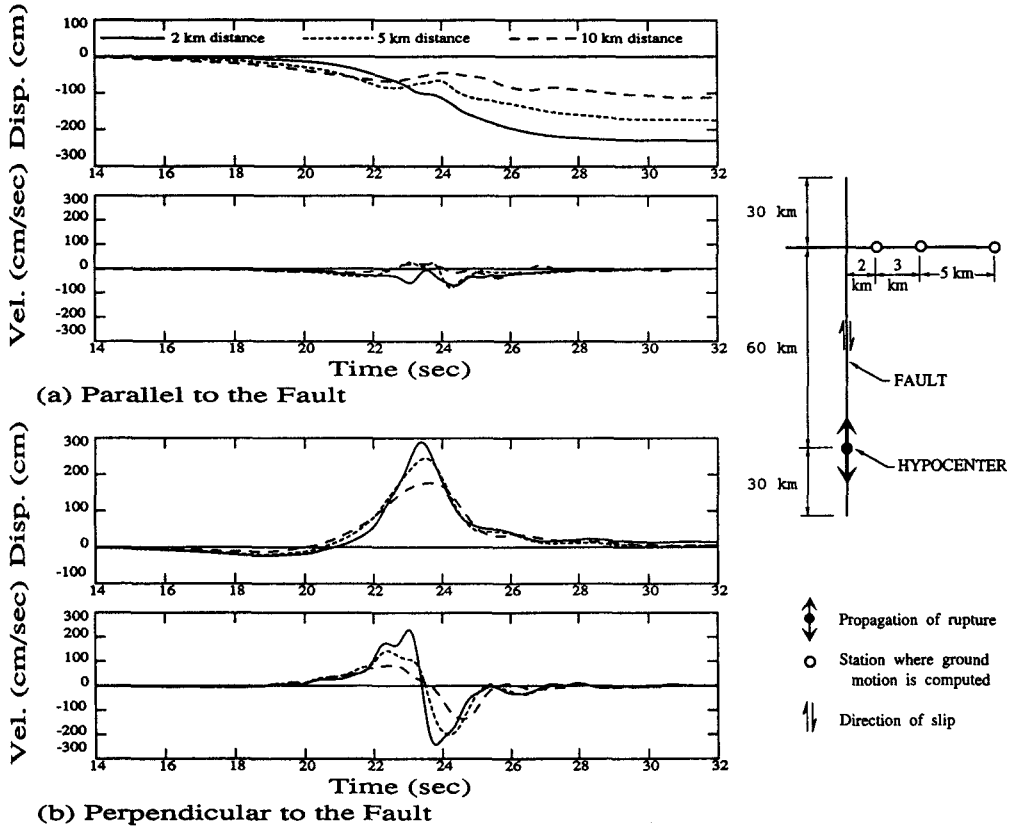

Figure 4 Simulated near-source ground motions for a M_W7.6 strike-slip earthquake (Hartzell and Heaton, 1990). Fault is vertical with a length of 120 km and a depth of 12 km.

For further information about ground motions in near-source regions, the reader is directed to recent reviews by Heaton and Hartzell (1988) and Somerville and Graves (1993).

SIMULATED GROUND MOTIONS FOR A M_W7.0 EARTHQUAKE

A M_W7.0 blind-thrust earthquake (Figure 5) is chosen as the subject event for the engineering simulations performed later in the paper. The fault dips 23° to the north in a vertically stratified crustal model that approximates the rock properties in the Los Angeles Basin. The rupture surface is 35 km long and 18 km wide and is confined to depths between 9 and 16 km. This mechanism is consistent with a possible M_W7.0 earthquake on the Elysian Park blind-thrust fault directly beneath Los Angeles (Figure 1). The earlier discussion indicates that the subject event is not a worst case and that it or a similar or even larger event somewhere in the Los Angeles region has enough likelihood of occurring that it should be considered by engineers.

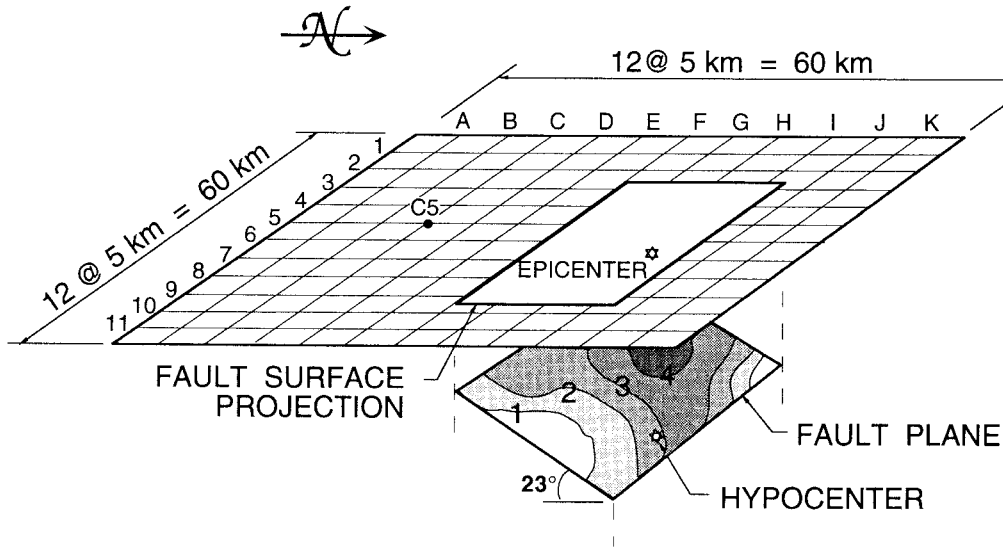

Figure 5 Details of the M_w7.0 earthquake simulation showing the dipping fault plane, contours of fault slip in meters, and 121 ground-surface sites where motions are computed.

Calculation of the ground motions uses different approaches for the long and short-period components. Motions at periods of 1 second and longer are computed deterministically as discussed below. The shorter periods are taken from actual existing records from the Northridge earthquake. A matched pair of filters is used to remove the short periods from the deterministically computed record and to remove the long periods from the actual record, and then the filtered records are summed to produce the final ground motion. The Northridge motions supplying the shorter periods are from the parking lot of the Olive View Hospital in Sylmar (Darragh, et al., 1994), used for locations in the direction of rupture (rectangular region bordered by line G on the north and line 06 on the east — see Figure 5), and from Stone Canyon Reservoir (U.C. Santa Barbara station), used elsewhere. These records are scaled according to the station location by an attenuation relation (Boore, et al., 1993) based on closest distance from the projection of the rupture onto the ground surface. The deterministic part of the ground motion is computed from point-dislocation solutions obtained in a layered half-space by discrete-wave-number finite-element techniques (Olson, et al., 1984) and is valid at periods of 1 second and greater. The assumed velocity distribution in the half-space is shown in Figure 6.

The slip distribution on the fault (Figure 5) is taken similar to that determined for the Homestead Valley segment in the 1992 Landers earthquake (Wald and Heaton, 1994a). Adjustments are made in rupture area (increased by a factor of 1.4) and fault slip (decreased by a factor of 0.74) to correspond to a M_w7.0 earthquake (Dolan, et al., 1995). Resulting average and peak slips are 2.2 m and 5.1 m, respectively. The velocity of the rupture is taken as 2.9 km/sec.

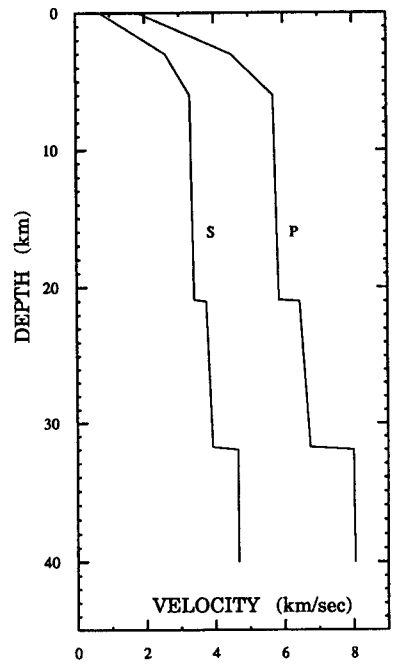

Figure 6 Assumed shear (S) and compression (P) wave velocity distributions with depth for the M_W7.0 earthquake simulation.

The slip-displacement history for a given point (x,y) adjacent to the fault which commences at time $t = t_0$ (corresponding to arrival of the rupture front) is assumed to be described by

$$u(x,y,t) = \tfrac{1}{2} D(x,y)\left[1 - e^{\left(\frac{-(t-t_0)}{\tau(x,y)}\right)}\left(1 + \frac{(t-t_0)}{\tau(x,y)}\right)\right]$$

where $D(x,y)$ is the final slip at the point (total slip from side to side) and $\tau(x,y)$ is a parameter that governs slip rate. This particle displacement function, which is shown in Figure 7, has a maximum particle velocity of 0.184 $D(x,y)/\tau(x,y)$ at time $t = t_0 + \tau(x,y)$. The displacement achieves 80% of its final value within the first $3\tau(x,y)$, and the average particle velocity is 0.133 $D(x,y)/\tau(x,y)$ within this time interval. This displacement function is the integral of Brune's (1970) far-field time function and is chosen for its smooth shape in the frequency domain. Although this displacement function differs from that derived from a model of a dynamically expanding crack, the difference is mostly in the high frequencies, which are filtered out anyway. The choices for $\tau(x,y)$ are 0.7 sec if $D(x,y) \geq 250$ cm and 0.5 sec if $D(x,y) < 250$ cm. Thus, the maximum particle velocity is on the order of 1m/sec, a value that is comparable to that derived for other earthquakes (Heaton, 1990).

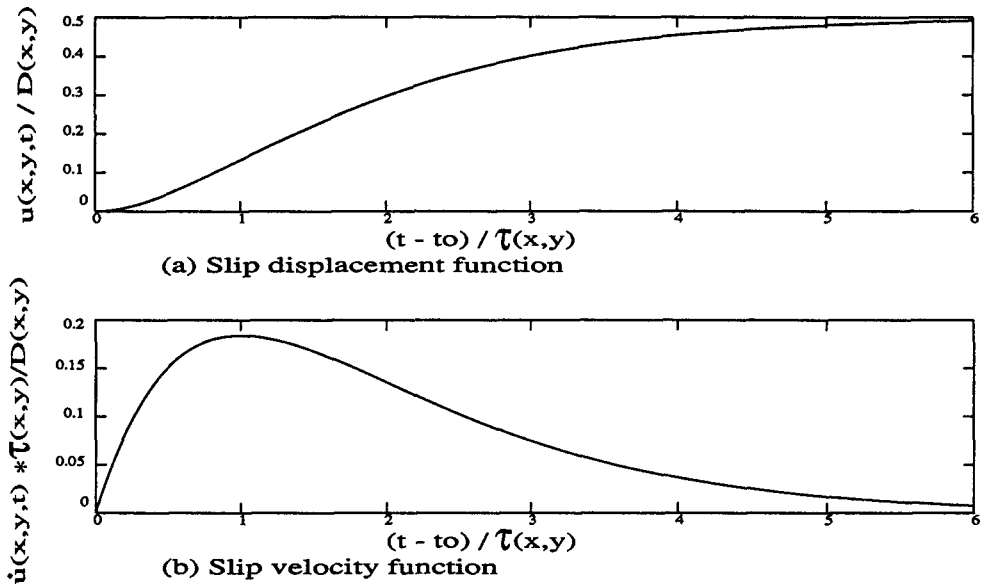

Figure 7 Particle displacement and velocity functions at the fault for the M_w7.0 earthquake simulation.

Ground motions are simulated on the rectangular grid of sites in Figure 5, 11 stations by 11 stations at a 5-km grid spacing covering 2500 km^2. Peak values of ground displacement and velocity over the entire region (Table 2) show largest values above and to the south of the fault where directivity dominates (peak displacement of 200 cm at D5, peak velocity of 180 cm/sec at H5). The area which experiences a peak displacement over 1 meter is about 600 km^2 in extent, and over most of this area the peak velocity exceeds 1 m/sec. The median of the peak velocities within 5 km of the surface projection of the fault rupture is 80 cm/sec, which is actually less than the median value of 103 cm/sec from Table 1. The large displacement pulses are of the shear-wave type and have both forward and back phases; this is seen in Figure 8 where the motion at C5 is plotted. In the above, the simulation results are reported for the component of ground motion at each station that maximizes the difference between the peak positive and negative velocities. These are the components used in the engineering analyses reported later.

A possible deficiency in the computation of the long-period motion is that multiple wave reflections within a 3-dimensional basin (such as the Los Angeles Basin) are not included. These effects, which contribute to the duration of shaking, increase in importance as the seismic source becomes shallower and larger. The simulated M_w7.0 earthquake is in a

TABLE 2

Peak ground displacement and velocity at 121 stations for the simulated M_w7.0 earthquake.

	1*	2	3	4	5	6	7	8	9	10	11	
K*	26.	28.	37.	47.	57.	56.	44.	34.	23.	12.	12.	
J	32.	32.	46.	70.	96.	96.	65.	48.	24.	17.	16.	
I	36.	34.	57.	95.	145.	134.	26.	59.	33.	21.	21.	
H	35.	36.	62.	109.	168.	152.	41.	67.	39.	33.	30.	Peak
G	37.	33.	60.	117.	176.	154.	71.	35.	39.	44.	39.	ground
F	36.	32.	63.	121.	182.	157.	75.	54.	45.	51.	45.	disp.
E	35.	31.	65.	129.	194.	183.	49.	58.	51.	58.	61.	(cm)
D	35.	32.	66.	128.	200.	164.	63.	74.	67.	73.	74.	
C	35.	34.	61.	117.	182.	150.	90.	69.	77.	83.	81.	
B	35.	36.	53.	96.	150.	146.	91.	67.	89.	88.	81.	
A	34.	36.	46.	75.	111.	117.	78.	54.	76.	79.	74.	

K	45.	44.	54.	47.	46.	40.	31.	27.	25.	21.	18.	
J	48.	54.	63.	72.	91.	66.	48.	37.	31.	31.	22.	
I	51.	87.	104.	122.	164.	110.	55.	43.	39.	33.	20.	
H	53.	87.	108.	96.	180.	117.	69.	47.	42.	35.	23.	Peak
G	49.	88.	92.	103.	174.	121.	78.	39.	46.	33.	26.	ground
F	49.	92.	78.	112.	158.	108.	66.	43.	46.	34.	25.	vel.
E	51.	96.	84.	119.	160.	125.	68.	53.	48.	35.	25.	(cm/sec)
D	52.	88.	78.	118.	158.	111.	76.	76.	58.	38.	27.	
C	50.	71.	65.	107.	139.	118.	85.	77.	59.	42.	32.	
B	51.	61.	64.	85.	115.	100.	78.	71.	58.	47.	34.	
A	47.	52.	56.	67.	82.	80.	85.	76.	60.	45.	33.	

*Station locations are shown in Figure 5.

range where the near-source pulse effect, of primary interest here, is likely dominated by direct shear waves that are determined primarily by source radiation and directivity effects, which are well modelled. However, duration of shaking is an important engineering parameter that also needs further study. The excitation of long-period surface waves in basins is discussed in more detail by Frankel (1993).

BASICS OF BUILDING RESPONSE TO GROUND-DISPLACEMENT PULSES

This section contains an analytical treatment of a building idealized as a uniform shear beam and subjected to two types of simple ground pulses. The purpose is to provide insight into building response to ground displacement pulses. One of the pulses is a forward only (nonreversing) displacement, denoted by *A* (Figure 9a), and the other is a forward and back (reversing) displacement, denoted by *B* (Figure 9b). The duration of displacement-pulse *B* is T_p, while that of pulse *A* is $\frac{1}{2}T_p$.

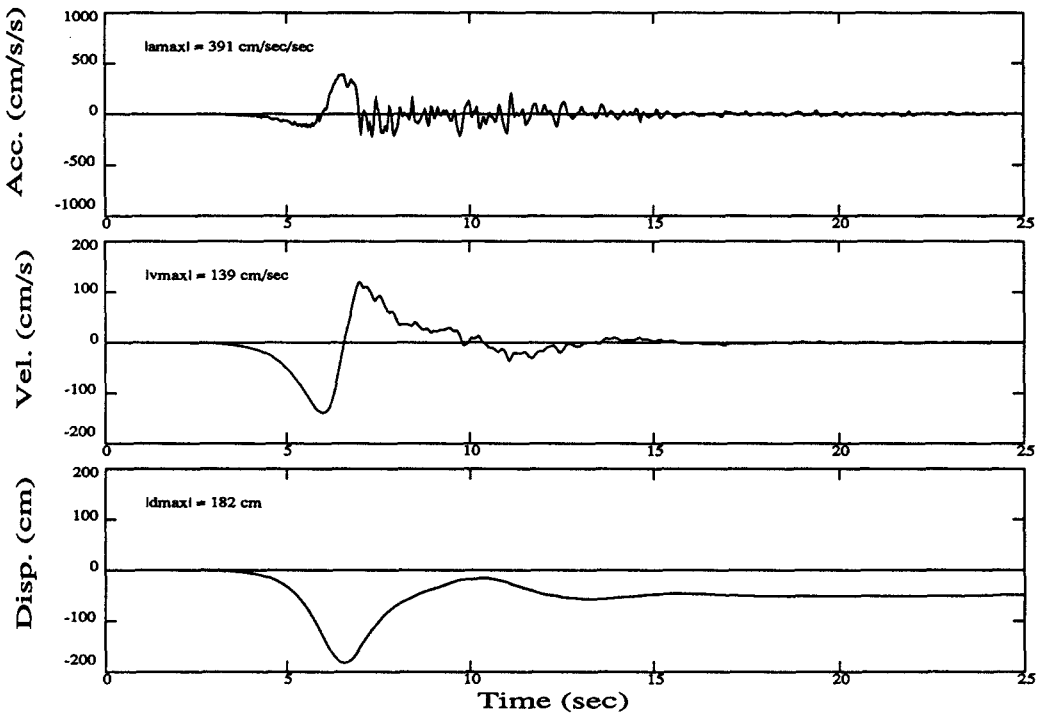

Figure 8 Simulated ground motions for the M_w7.0 earthquake at location C5 for orientation N36°E.

Linearly-elastic behavior is investigated first. The shear building (Figure 10) has mass per unit height ρ, shear stiffness per unit height G, and shear-wave speed $C = \sqrt{G/\rho}$. Damping is omitted. If the shear building has infinite height, the shear strain $\gamma(y,t)$ at an elevation y is given by

$$\gamma(y,t) = \frac{-v_g(t - y/C)}{C} \quad ;$$

i.e., the ground velocity $v_g(t)$ produces a shear-strain wave whose amplitude is proportional to the ground velocity and which travels up the building.

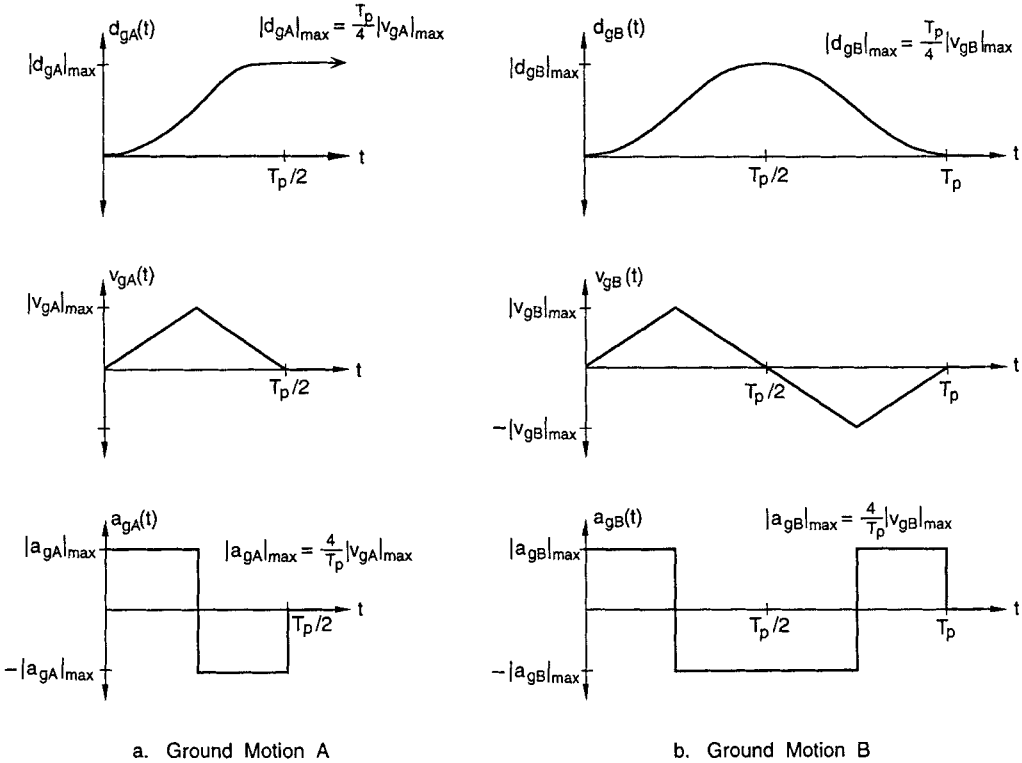

a. Ground Motion A b. Ground Motion B

Figure 9 Simple pulse-type ground displacement motions A (forward motion only) and B (forward and back motion).

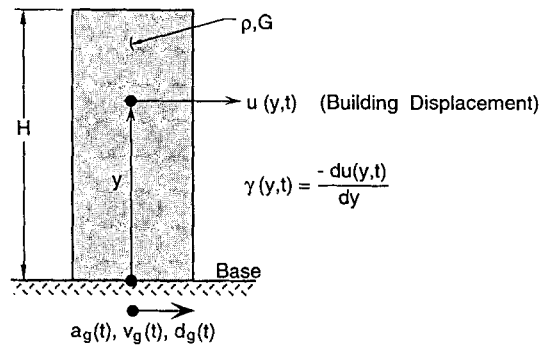

Figure 10

Idealized multi-story building modelled as an elastic shear beam.

For a shear building of finite height H, the strain $\gamma(y,t)$ is the sum of contributions from the initial wave and all subsequent reflections up to time t. A strain wave reflects with opposite sign off the top of the building and with the same sign off the building base. At the base of the building, the shear strain [denoted by $\gamma^b(t)$] is

$$\gamma^b(t)=\left[-v_g(t)+2v_g\left(t-\frac{2H}{C}\right)-2v_g\left(t-\frac{4H}{C}\right)+\cdots\right]\frac{1}{C} \quad ,$$

which applies for an arbitrary ground velocity $v_g(t)$.

Of interest is the maximum shear strain at the base

$$\left|\gamma^b\right|_{\max}=\frac{\left|v_g\right|_{\max}}{C}\mathcal{A}$$

where $\mathcal{A}$ is an amplification factor. For ground motions A and B, $\mathcal{A}$ depends on T_p / T_1 where $T_1 = 4H / C$, the fundamental period of the shear building. The factor $\mathcal{A}$ reaches 2 for ground motion A (when $T_p \leq T_1$) and 4 for ground motion B (when $T_p = T_1$). Plots of $\gamma^b(t)$ for $T_p = T_1$ are shown in Figure 11, and configurations of the building at the six times $t = 0$, $T_p/4$, $T_p/2$, $3T_p/4$, T_p and 5/4 T_p are shown in Figures 12a and 12b.

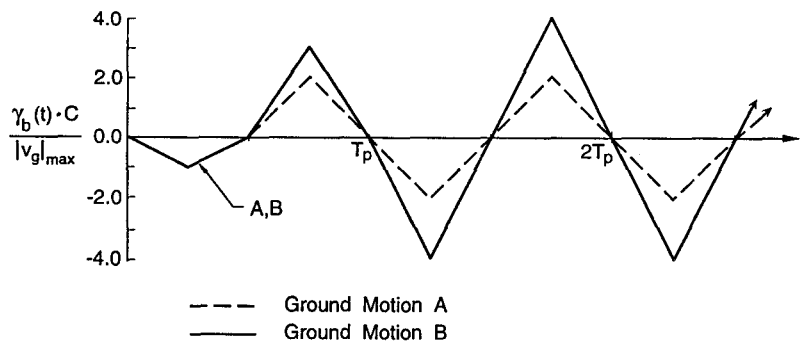

Figure 11 Shear-strain time histories at the base of the elastic shear-beam building from ground motions A and B for the case $T_p = T_1$.

The shear strain $\left|\gamma^b\right|_{\max}$ can be large enough to be well into the inelastic range. With $\left|v_g\right|_{\max}$ = 1 m/sec and C = 100 m/sec (a typical value for a multi-story building), $\left|\gamma^b\right|_{\max}$ = $\mathcal{A}$/100 which gives $\left|\gamma^b\right|_{\max}$ = 0.02 for ground motion A and 0.04 for ground motion B, when $T_p = T_1$. These are large values and can greatly exceed the yield strain γ^b_{yld} at the base of the building

$$\gamma^b_{\text{yld}}=\frac{\alpha\rho gH}{G}$$

where g = acceleration of gravity, and α is a lateral force coefficient which gives the shear strength at the base of the building when multiplied by the building weight ρgH. The value of α necessary for the behavior to be elastic is obtained by equating $\left|\gamma^b\right|_{\max}$ and γ^b_{yld} as

$$\alpha_{\text{elas}} = \frac{4\mathcal{A}|v_g|_{\max}}{T_1 g}$$

With $|v_g|_{\max}$ = 1 m/sec, g = 9.8 m/sec and T_1 = 3 sec, α_{elas} equals 0.27 for ground motion A ($\mathcal{A}$= 2) and 0.54 for ground motion B ($\mathcal{A}$ = 4). For an actual multi-story building, α is typically 0.1 or less, indicating that inelastic behavior will occur for even moderate values of $|v_g|_{\max}$. For a given value of $|v_g|_{\max}$, inelastic effects will be more important for the forward and back pulse (ground motion B) because of the greater response that it produces. Inelastic effects could cause $|\gamma^b|_{\max}$ to greatly exceed the above estimates of 0.02 for ground motion A or 0.04 for ground motion B.

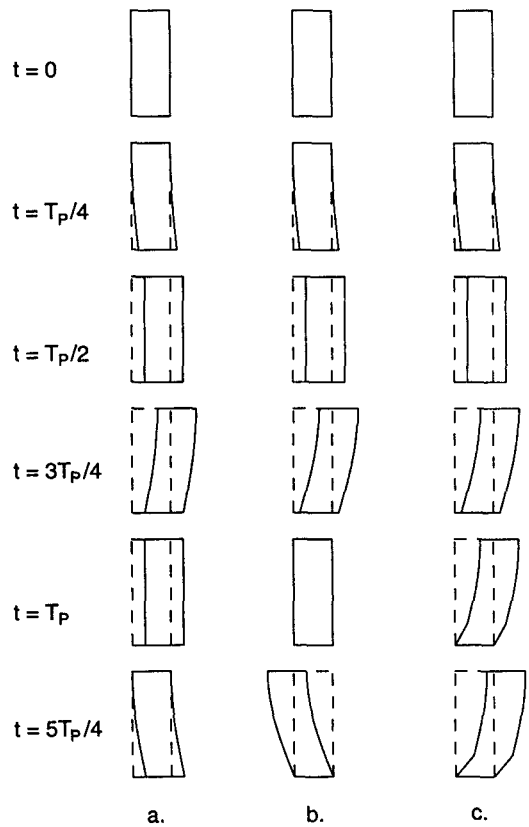

Figure 12 Configuration of a multi-story building at time intervals of $T_p/4$ for the case $T_p = T_1$. a) Elastic shear-beam building for ground motion A. b) Elastic shear-beam building for ground motion B. c) Inelastic shear-beam building for ground motion B (qualitative depiction).

One scenario involving ground motion B which could cause severe deformation in a building is for the building to acquire a large forward velocity by the time the ground stops moving after its forward phase at $t = T_p/2$, which would happen as long as the building is strong enough to avoid excessive yielding over $0 \leq t < T_p/2$, and then have a yield mechanism form in the lower part of the building for $t > T_p/2$ as the building continues to move forward and the ground is moving back. To relate this to wave propagation in the building, the back phase of the ground displacement pulse, which creates a negative shear strain γ, occurs as the negative reflection of γ off the top of the building arrives and doubles at the base. The scenario is illustrated in Figure 12c. Because the building responds more slowly when it yields, a ground motion having a T_p exceeding the building's elastic period may be the most severe, unlike the elastic case for which $T_p = T_1$ is most severe. In addition to the timing, the strength of the pulse as measured by both displacement and velocity is very important. A pulse displacement of 1 or 2 meters, especially of the forward and back (reversing) type, with a peak velocity of 1 m/sec would be quite severe.

RESPONSE OF 20-STORY STEEL-FRAME BUILDING

The seismic design provisions in the Uniform Building Code (International Conference of Building Officials, 1991, 1994) are taken from the SEAOC Blue Book (Seismology Committee of the Structural Engineers Association of California, 1990) where it is stated that the intention of the provisions is to prevent collapse under ground motions having an "intensity equal to the strongest either experienced or forecast for the building site," which has been quantified as a 500-year event. According to the Blue Book, for this event, damage will occur but it is expected to be repairable. However, this view is at odds with findings (Bertero, et al., 1978; Anderson and Bertero, 1987) that near-source pulse-like ground motions, such as present in some of the records from the 1971 San Fernando and 1979 Imperial Valley earthquakes, can place severe inelastic demands on multi-story buildings. Furthermore, the near-source features of the ground motions presented in this paper for the simulated M_w7.0 earthquake are stronger than those considered in the earlier research and would be expected to have even more severe effects.

The building considered is 20 stories tall with a rectangular plan and two axes of symmetry (Figure 13). Moment-resisting frames exist on the perimeter only, and all interior connections are simple. Design meets the 1991 and 1994 Uniform Building Codes for gravity loads [floor live load = 3.8 kPa (80 psf), floor dead load = 4.5 kPa (95 psf), roof dead load = 3.8 kPa (80 psf), exterior cladding load = 1.7 kPa (35 psf)], wind [basic wind speed = 113 kph, urban exposure (B)] and earthquake [Zone 4, deep stiff soil (Type S_2)]. For seismic design, the resulting code base-shear coefficient V/W = 0.03. Steel grade is A36. Where necessary, the panel zones are strengthened with doubler plates so that the panel-zone yield moment equals 0.8 times the sum of the plastic moment capacity of the connecting beams. This building has been strengthened compared to the original one considered in previous analytical studies (Tsai and Popov, 1988; Challa and Hall, 1994; Heaton, et al., 1995) in order

to reduce the wind drift in the lower stories from about 0.0030 to 0.0025. This drift is accomplished without the inter-story shear springs mentioned below.

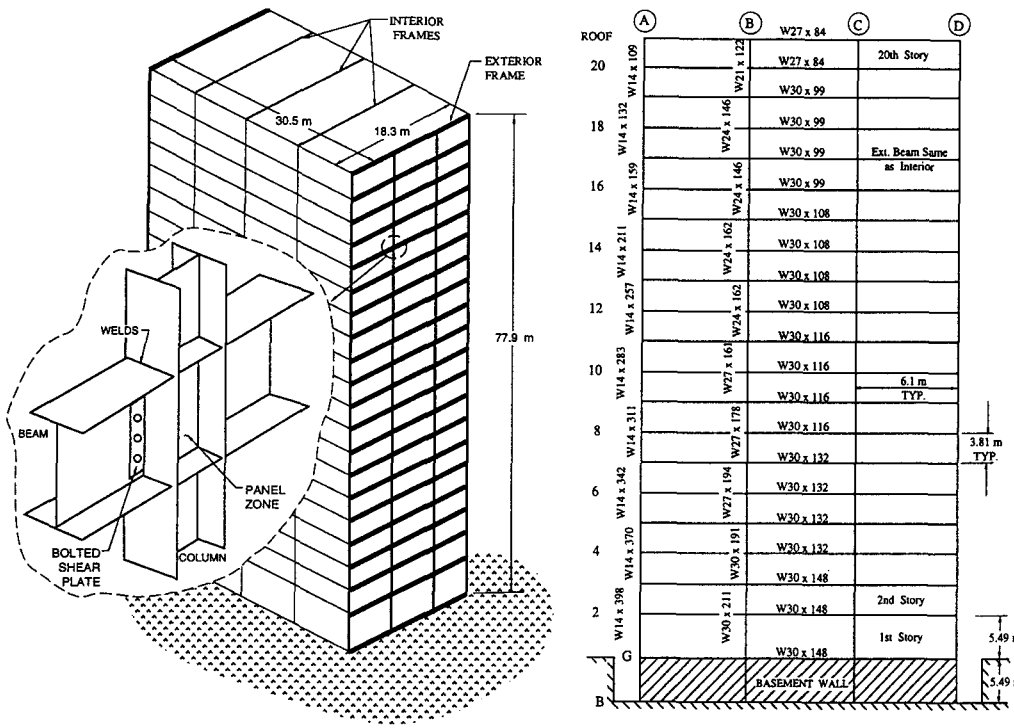

Figure 13 Twenty-story steel-frame building used in the computer simulation study. Left: perspective view of the building with detail of the beam-column joint shown in the inset. Right: Details of the end frame at the narrow face of the building (not drawn to scale). Inter-story shear springs and foundation springs are not shown.

Several simplifying assumptions – namely: applying the ground motion only as a single horizontal component in the short direction of the building, neglecting 3-dimensional frame action, neglecting in-plane flexibility of the floor slabs, and enforcing symmetry (even in the nonlinear response range) – permit the building to be represented as 2½ parallel frames (one exterior and 1½ interior, parallel to the short direction of the building) which deflect only in-plane with equal lateral displacements across each floor level. The exterior frame (Figure 13) is modelled by the fiber method (Challa and Hall, 1994) whereby each beam or column member is divided along its length into subelements, and each subelement is divided within its cross-section into axial fibers (Figure 14). Panel zones are modelled as shear elements. The 1½ interior frames are not modelled explicitly, but are included as shear springs which connect adjacent floors of the exterior frame. These shear springs are also intended to represent additional contributors to the lateral stiffness and strength of the building from nonstructural elements. Half the mass of the building (including live load of

0.48 kPa) is distributed to the horizontal degrees of freedom of the exterior frame; masses and gravity loads for the vertical degrees of freedom of this frame (including live load of 0.72 kPa) are from a ½-bay tributary width. Foundation interaction is included by the use of axial-spring supports, one horizontal and one vertical, at the base of each column. Very stiff wall elements are used in the below-ground story to simulate the presence of basement walls. The complete building model has a fundamental period of vibration of 3.48 seconds in the elastic range.

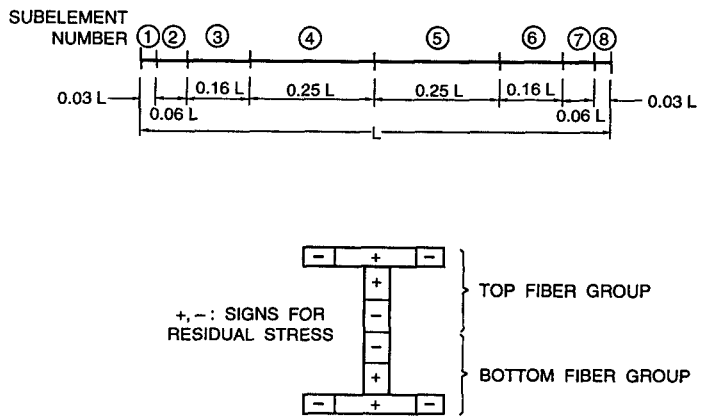

Figure 14 Details of beam-column modelling showing longitudinal distribution of subelements (top) and arrangement of fibers within the cross-section (bottom).

The mathematical model contains a variety of nonlinear features. Realistic hysteretic axial stress-strain behavior, using steel strengths of 290 MPa (42 ksi) yield and 448 MPa (65 ksi) ultimate, is incorporated for each fiber in the beams and columns (Challa and Hall, 1994). The fiber residual stress is ±41 MPa (6 ksi); see Figure 14. Realistic hysteretic behavior is also used for the panel zones where the deformation mechanism is one of shear (Challa and Hall, 1994). The inter-story shear springs are elastic-perfectly plastic (Figure 15) and provide a strength F_{yi} in story i equal to the story shear produced by the code earthquake design forces for a lateral-force coefficient of 0.01 of the building weight. The stiffness k_i of the shear spring in story i is computed as F_{yi} /0.0025 h_i where h_i is the height of story i. An elastic-plastic-with-hardening relation (Figure 15) is used for the vertical foundation springs, while the horizontal ones are taken to be elastic. (In the analyses, the vertical foundation springs carry much higher force than the horizontal ones.) The above material nonlinearities provide energy dissipation through hysteresis. Geometric nonlinearity (P-Δ effects and moment amplification) is accounted for in the exterior frame through configuration updating. P-Δ effects from the interior building weight are handled by applying lateral loads to the exterior frame which are computed from the interior gravity loads and the current story offsets.

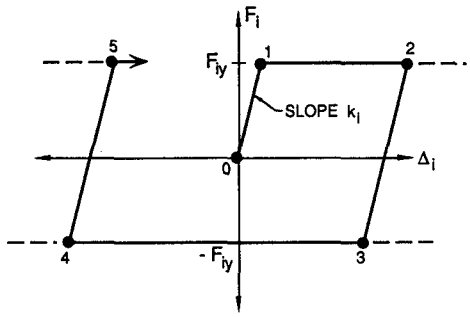

Story i	k_i kN/cm (kips/in)	F_{iy} kN (kips)
1	344 (196)	328 (73.7)
2	342 (195)	326 (73.3)
•	•	•
•	•	•
19	114 (65.2)	109 (24.5)
20	89.2 (50.9)	85.0 (19.1)

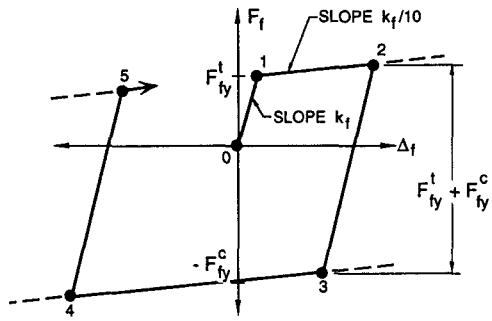

Horizontal spring (elastic)

k_f = 5254 kN/cm (3000 kips/in)

Vertical spring

F^t_{fy} = 6.67 MN (1500 kips)

F^c_{fy} = 13.3 MN (3000 kips)

k_f = 5254 kN/cm (3000 kips/in)

Figure 15 Details of inter-story shear springs (top) and foundation springs (bottom) for the 20-story building. For a shear spring in story i, F_i = force carried, F_{iy} = yield strength, Δ_i = displacement, and k_i = initial stiffness. For a foundation spring, F_f = force carried, F^t_{fy} = tension yield strength, F^c_{fy} = compression yield strength, Δ_f = displacement, and k_f = initial stiffness.

Viscous damping is added as two stiffness-proportional terms. The first is the total linear stiffness matrix multiplied by the factor $2\xi' T_1 / 2\pi$, where $\xi' = 0.005$ and $T_1 = 3.48$ sec. The second corresponds to dampers parallel to the inter-story shear springs, with damping value in story i equal to $(2\xi'' T_1 / 2\pi) 5k_i$, where $\xi'' = 0.05$. Limits are imposed on the forces carried by the story dampers because high relative velocities occurring after yielding can otherwise cause unrealistically high damping forces. The force capacity of a story damper is set to the inter-story shear-spring strength F_{yi}, which gives significant damping.

No structural degradation such as flange buckling or weld fracture (as seen in the Northridge earthquake, Bertero, et al., 1994) is included, except for one analysis discussed later. The fiber method lends itself well to representing some features of weld fracture, and this subject will be studied in more detail in future work.

Because of the many assumptions, some conservative and some not, made in formulating the mathematical model, interpretation of the results must be done carefully. Also, some of the results presented here may be applicable to a concrete-frame building since the

design force levels for steel and concrete are similar. Generalizations to buildings of other heights should consider that shorter buildings are designed with higher seismic coefficients and that the strengths of taller buildings are significantly increased because of wind-load considerations, so buildings of intermediate height, such as the 20-story building analyzed here, may have relatively less lateral strength than those of other heights.

Response of the 20-story building is examined first for two ground motions: that recorded in the parking lot of the Olive View Hospital in Sylmar during the Northridge earthquake (Darragh, et al., 1994) and that at site C5 (Figure 8) for the simulated M_w7.0 earthquake. The Sylmar motion, because of its high accelerations, velocities and long-period content, ranks as one of the highest in terms of damage potential ever recorded. This analysis, which employs the N-S component of the Sylmar motion, will serve as a reference. For the simulated earthquake, the C5 motion is not the strongest but should be among the most severe based on its peak ground displacement (182 cm) and velocity (139 cm/sec). The C5 displacement pulse is of the forward and back type, although the return is incomplete by about 20 cm.

Elastic response spectra for the two ground motions are shown in Figure 16. Attenuation of the high frequencies in the C5 motion, compared to Sylmar, is evident. However, high frequency content is mostly irrelevant as far as the response of the long-period structures considered here is concerned. The long-period content of the Sylmar motion is high compared to most recorded ground motions, but it is exceeded by that of the C5 ground motion beyond a period of 1.7 seconds. Also shown in Figure 16 is the UBC earthquake representation for soil type S_2 which has been adjusted upward by a factor of 1.7/1.33 to account for load factors. In the long-period range, the C5 curve is considerably higher than the UBC, but Sylmar is smaller. While such a comparison provides some indication of the collapse or damage potential of these ground motions, this potential for the C5 motion may be even higher than suggested by its elastic response spectrum since the motion contains a large, rapid displacement pulse that can push a structure far into a nonlinear excursion.

Two types of output are presented. First are time histories of horizontal response of all of the floors and the roof which are plotted as total displacements (not relative to the ground). Second are charts of nonrecoverable (plastic) rotation for hinge regions in beams and columns. A rotation capacity of 0.015 to 0.025 radians without significant deterioration is considered acceptable, although this is often difficult to achieve, even in laboratory tests (Engelhardt and Husain, 1993). Plastic shear strains in the panel zones are also included in the charts.

While significant inelastic behavior occurs for the N-S Sylmar ground motion, the amount is not excessive. The peak story drift is 1.4% while peak plastic rotations are 0.008 radians in a second-floor beam and 0.006 radians in a column just above the ground floor. Column plastic hinges at this location are expected because of the high lateral stiffness of the story below. One characteristic of the building response is large overturning forces. The maximum net tension occurring in an exterior 1st-story column is 4.9 MN (1100 kips). For

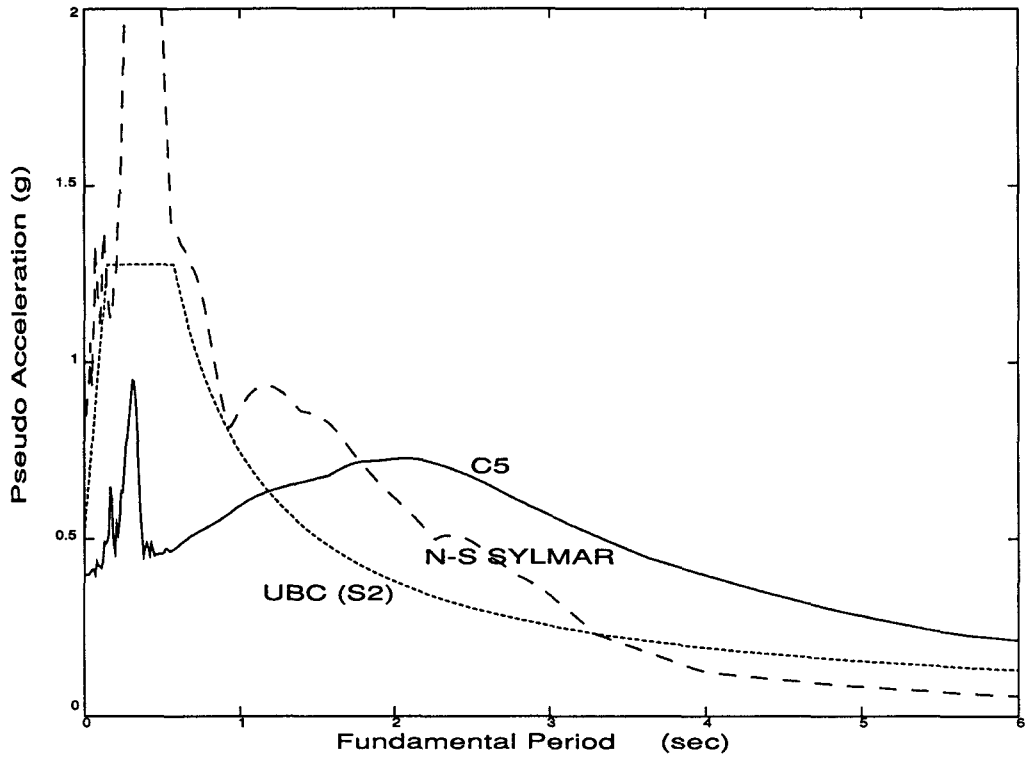

Figure 16 Pseudo-acceleration response spectra for ground motions C5 and Sylmar. Also shown is the UBC spectrum for soil type S_2 scaled up by 1.7/1.33.

reference, the gravity load carried by this column is 2.8 MN (640 kips) compression, and the axial yield force in the column is 21.9 MN (4910 kips).

The C5 ground motion produces a more severe response as shown in Figures 17 and 18. The peak story drift is 5.9% while peak plastic rotations are 0.051 radians (beam) and 0.024 radians (column); the peak shear strain in a panel zone is 0.007 radians. A perspective view of the building configuration is shown in Figure 19 with lateral displacements multiplied by four. The response to the forward and back displacement pulse is similar to that shown in Figure 12c and discussed in the previous section, although the largest story drifts occur at about the one-third height of this 20-story building.

The amount of yielding produced by the C5 motion is large enough for considerable structural deterioration (not included in the analysis) to occur, even assuming all welds hold, and so collapse can not be ruled out. One possible collapse scenario would involve excessive lateral displacements in some of the stories aided by the weight of the building acting through the large story offsets (P-Δeffects). Such a collapse mechanism requires column hinging, and, as seen in Figure 19, plastic rotations in the columns do occur even though the code requirement that column strength exceed beam strength is satisfied. Large overturning forces generated by the C5 ground motions are also a concern. At the 1st-story exterior columns,

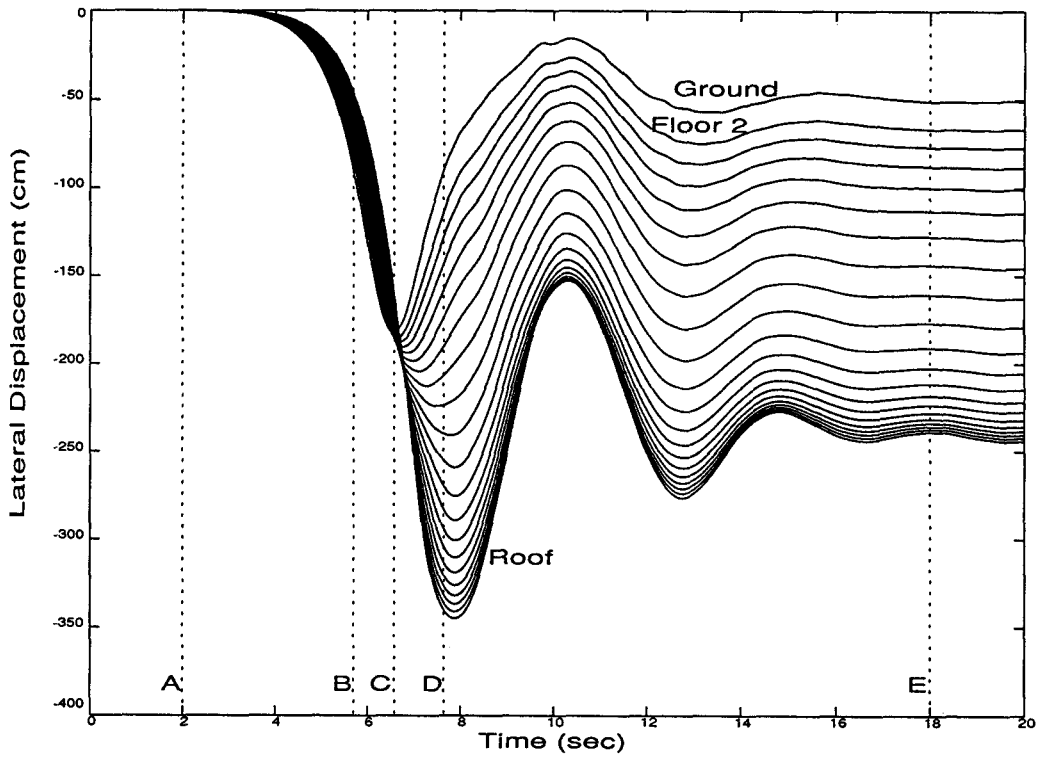

Figure 17 Lateral-displacement time histories at ground, all floors and roof of the 20-story building for the C5 ground motion.

peak axial net forces reach 9.8 MN (2190 kips) tension and 14.7 MN (3300 kips) compression, and these forces are limited by foundation yielding.

In order to assess how the 20-story building would fare if located arbitrarily in the 50 km × 50 km region where the ground motions were simulated, the analysis is repeated for each of the 121 grid points (total of 29 CPU hours on a DEC 3000 Model 400 with a 100 MIPS processor). Peak responses at the 121 sites are given in Table 3 in terms of the largest drift in any story. Site D5 produces the largest story drift (6.4%) as well as the largest plastic beam rotation (0.056 rad) and column tension (10.2 MN). The region of severe inelastic deformation, defined, say, by a story drift above 3%, covers on the order of 500 km^2. The region where high column tensions occur is much larger and extends beyond the region of the simulation.

Based on the Northridge experience, one would expect weld fractures in the beam-to-column connections to play an important role in the building responses computed above. Column cracks (also observed in the Northridge earthquake) and column-splice failures could perhaps be of even greater importance when overturning forces are large. The potential

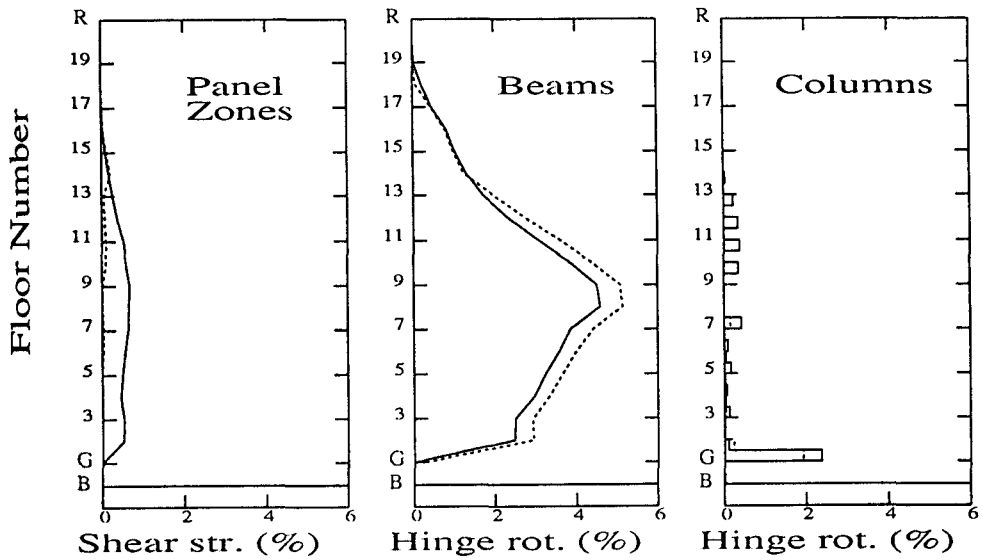

Figure 18 Peak values for panel-zone plastic shear strains and for beam and column plastic-hinge rotations in the 20-story building for the C5 ground motion. Shear strains and hinge rotations are given in %, i.e., radians × 100. Solid lines are for joints along column lines A and D (exterior), and dotted lines are for joints along column lines B and C (interior).

Figure 19

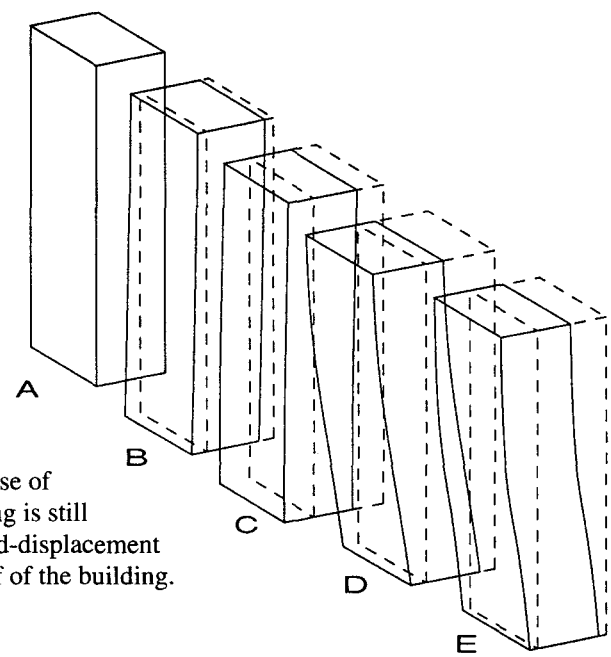

Perspective view of the 20-story building responding to the C5 ground motion at the times A, B, C, D and E marked in Figure 17. A: Building is at rest before ground displacement pulse arrives. B: Forward phase of the pulse. Building is moving forward, but lagging in the upper stories. C: Ground has reached its maximum displacement. Most of the building is moving rapidly forward. D: Back phase of the pulse. Upper portion of the building is still moving forward. E: End of the ground-displacement pulse. Offsets remain in the lower half of the building.

TABLE 3

Peak responses of the 20-story building to the M_w7.0 ground motions at the 121 stations: largest drift in any story

	1	2	3	4	5	6	7	8	9	10	11
K	0.9	0.9	0.9	1.1	1.1	0.8	0.6	0.5	0.4	0.3	0.2
J	1.0	0.9	1.2	2.2	2.6	1.6	0.8	0.7	0.4	0.4	0.2
I	1.1	1.0	2.0	2.6	4.1	2.9	1.1	0.8	0.5	0.4	0.2
H	1.0	0.9	2.1	3.4	5.2	3.4	1.9	0.9	0.7	0.5	0.3
G	0.9	0.8	1.8	3.7	5.3	3.1	2.5	0.4	0.6	0.5	0.2
F	0.9	0.8	1.7	3.8	5.4	3.2	1.4	0.7	0.7	0.5	0.2
E	1.0	1.0	1.8	4.2	6.0	4.0	1.4	0.9	0.6	0.4	0.3
D	1.0	0.9	1.8	4.2	6.4	4.3	1.4	1.3	0.7	0.4	0.2
C	0.9	0.9	1.8	3.6	5.9	4.0	2.0	1.5	0.8	0.4	0.2
B	0.9	0.9	1.2	2.6	4.3	3.3	1.9	2.0	0.9	0.5	0.3
A	0.9	0.9	0.8	1.9	2.7	2.7	1.8	2.4	1.5	0.6	0.3

Peak drift in any story (%)

effects of weld fracture on the response of the 20-story building can be demonstrated by giving certain fibers the property of fracturing (loss of tensile capacity) when the fiber axial stress reaches some critical value. This property is assigned only to fibers at weld locations: beam subelements 1 and 8 for beam-to-column welds (fibers in all bottom fiber groups and in a random 25% of top fiber groups) and column subelement 4 just below mid-height in the 1st, 3rd, 5th, etc. stories for column-splice welds. (See Figure 14 for an explanation of the terminology.) For the beam-to-column welds, the critical fracture stress is set to the yield stress; compression can be carried when contact is regained; and shear stiffness is maintained even if all fibers at subelements 1 or 8 fracture. Behavior in subelement 4 for column-splice welds is similar except that the critical fracture stress is set to the yield stress (column lines A and D) or 2/3 of the yield stress (column lines B and C) and all load-carrying capability is permanently removed from a column after all fibers in subelement 4 fracture. The reason for the reduced fracture stress at the column splices along lines B and C is to account for the presence of partial penetration welds.

The computed response to the N-S Sylmar motion, with weld-fracture capabilities included, shows only beam-to-column fractures as the overturning effects are greatly reduced compared to the case where weld fractures are prevented. The building does not collapse and the residual lateral displacement at the roof is 13 cm (compared to a value of 3 cm if all weld fractures are prevented), and this is in line with experience from the Northridge earthquake. Computations for the C5 ground motion eventually encounter convergence difficulties but are sufficient to show that the building collapses (Figure 20). The forward momentum acquired during the initial phase of the ground-displacement pulse produces many weld fractures and excessive story drifts. Figure 21 shows the distribution of weld fractures in the frame at time 14 seconds in the simulation. Both column-splice fractures and beam-to-column fractures occur. Those at column splices result primarily from bending as the column axial forces from overturning are again greatly reduced by fractures in the beam-to-column connections; the maximum net tension in an exterior 1st-story column is 3.5 MN (790 kips).

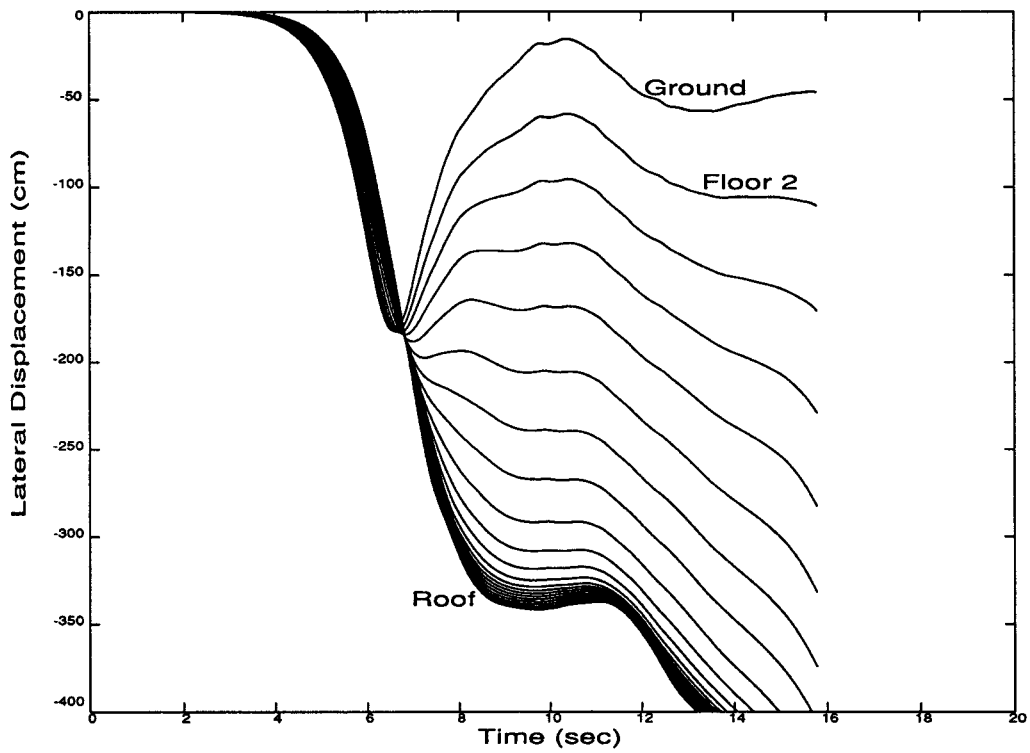

Figure 20 Collapsing response of 20-story building to C5 ground motion with weld fractures allowed. Rules for weld fracture are described in the text. The analysis is carried to the point where convergence difficulties occur.

The rules used for weld fracture in the above simulation, although reasonable, are arbitrary. Within the range of rules considered to be reasonable, there can be a considerable variation in the building's response. For example, in the results presented for the C5 motion, none of the columns lost axial capacity, but lower splice strengths would have allowed some splices to fracture all the way through.

Other preliminary analyses have been run with composite slab action represented through an equivalent fiber at the top of the beams. This increases the beam bending strength which results in more column hinging, and so no reduction in story drifts and potential for collapse was observed.

THREE-STORY BASE-ISOLATED BUILDING

An important application of base-isolation has been for structures which should remain functional during and following earthquakes. A major concern in the design of a base-isolated building is to accommodate large displacements across the isolators which could occur during strong long-period ground shaking from a major earthquake, including a

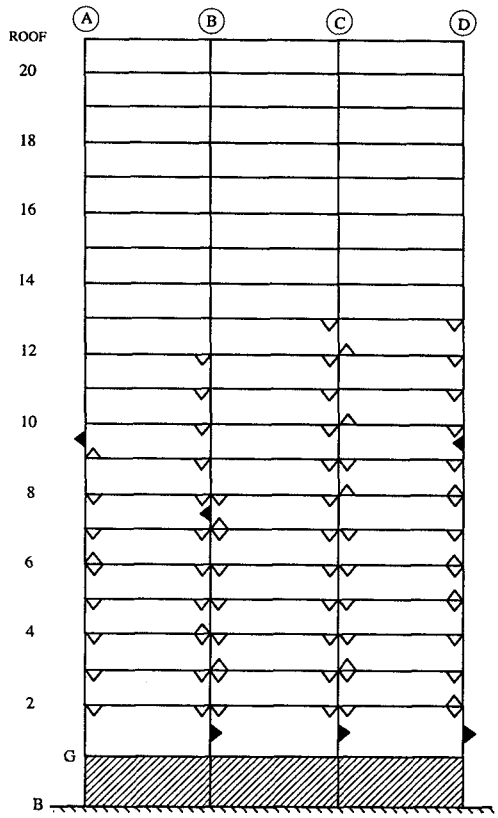

Figure 21

Distribution of weld fractures at time 14 seconds for the response shown in Figure 20. A dark triangle locates a cracked column-flange weld at a column splice, while an open triangle locates a cracked beam-flange weld at a beam-to-column connection. Frame not drawn to scale.

large rapid ground-displacement pulse (especially a reversing one) in the near-source region. Excessive displacements across the isolators could damage the building through failure of the isolators or resulting from impacts between the building and its perimeter walls or other barrier systems which define the zone of free movement (moat).

The system considered (Figure 22, Table 4) is an idealized 3-story shear building (floor masses connected by inter-story shear springs) mounted on flexible pads and subject to a single horizontal component of ground motion. Three moat widths (taken equal to the total maximum pad displacement, D_{TM} in the UBC) are examined: 40 cm, 50 cm and 60 cm. The 40-cm clearance is comparable to or somewhat greater than that used in several existing Southern California buildings, while 60 cm is about the largest D_{TM} that is currently being used for designs located close to major faults. All the isolator designs have fundamental periods (T_I in the UBC) of 2.25 sec and an amount of energy dissipation associated with hysteretic action of the pads when cycled at the design displacement (D in the UBC, taken here as $\frac{2}{3} D_{TM}$) equivalent to viscous damping (B in the UBC) at 15% of critical. Quantification of the fundamental period and the equivalent viscous damping refers to a mass-spring oscillator whose mass equals that of the building above the pads and whose stiffness equals the secant stiffness of the pads at the design displacement. The force-displacement relation for the pads (all pads combined) is bi-linear with a cap as defined in Figure 22 and Table 4.

In addition, the benefit of augmenting the energy dissipation in the pads with viscous damping (B') at 5% or 10% of critical is examined. Thus, a total of nine isolation designs are considered: 40/0, 40/5, 40/10, 50/0, 50/5, 50/10, 60/0, 60/5, 60/10, where the first number is D_{TM} in cm and the second is B' in % of critical. The addition of dashpots alongside the pads is being used in current practice for near-fault locations. Results for the fixed-base building (same building but no pads) are also presented.

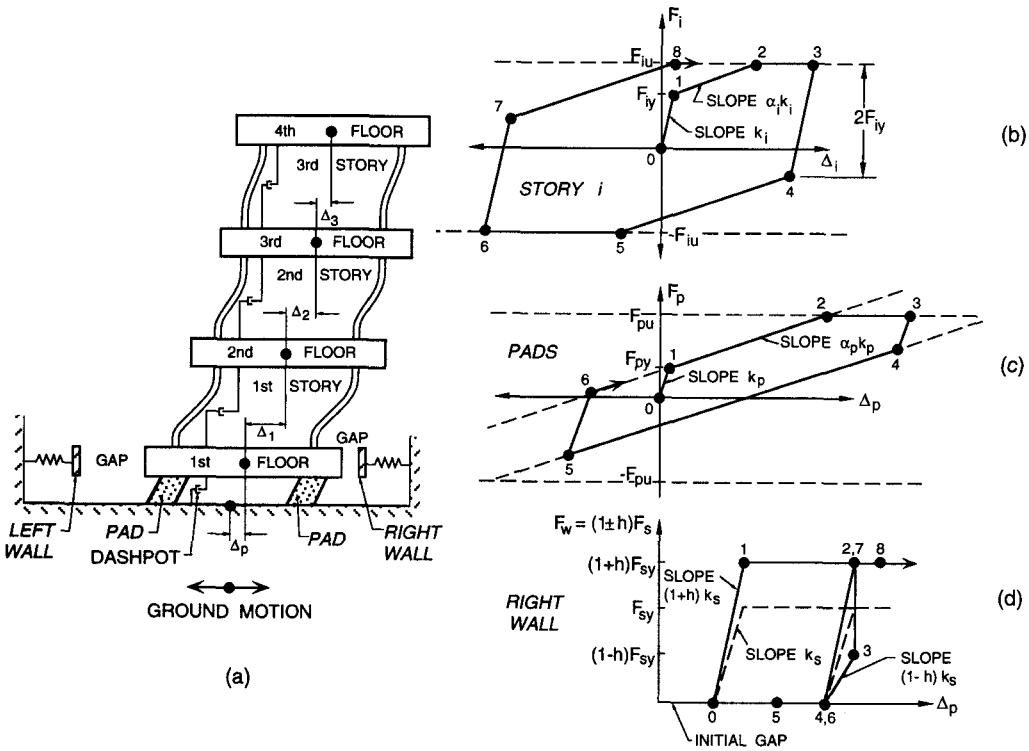

Figure 22 Details of idealized 3-story base-isolated shear building used in computer simulation study. Hysteretic behavior is defined at right for the ith-story of the building (top), all of the pads combined (middle), and the right wall (bottom; left wall similar). For story i, F_i = force carried, F_{iy} = yield strength, F_{iu} = ultimate strength, Δ_i = displacement, k_i = initial stiffness, and α_i = ratio of secondary to initial stiffness. For the pads, F_p = force carried, F_{py} = yield strength, F_{pu} = ultimate strength, Δ_p = displacement, k_p = initial stiffness of pads, and α_p = ratio of secondary to initial stiffness of pads. For a wall, F_w = force carried (plus spring hysteretic damper), Δ_p = pad displacement (equal to displacement of 1st floor relative to ground), F_s = force carried by spring, F_{sy} = spring yield strength, k_s = initial stiffness of spring, and h = hysteretic damping coefficient. Values for the dashpot located alongside the pads are discussed in the text.

TABLE 4

Properties of 3-story base-isolated building.

Building

m_1 = 999 tonnes* (2200 kips weight)

m_2 = 817 tonnes (1800 kips weight)

m_3 = 817 tonnes (1800 kips weight)

m_4 = 636 tonnes (1400 kips weight)

k_1 = 6339 kN/cm (3620 kips/in)

k_2 = 4437 kN/cm (2534 kips/in)

k_3 = 2536 kN/cm (1448 kips/in)

α_i = 0.1 i = 1,2,3

F_{1y} = 4448 kN (1000 kips)

$F_{iy} = F_{1y}\,(k_i / k_1)$ i = 2,3

$F_{iu} = 1.4\,F_{iy}$

Damper at pads

B' = 0%, 5%, 10%

Barrier walls

k_s = 8,756 kN/cm (5,000 kips/in)

F_{sy} = 22,240 kN (5000 kips)

h = 0.6

Initial moat width = D_{TM}

Pads

k_p = 1272 kN/cm (726 kips/in) α_p = 0.15

F_{py} = 1999 kN (449 kips) for D_{TM} = 40 cm; 2499 kN (562 kips) for D_{TM} = 50 cm; 2998 kN (674 kips) for D_{TM} = 60 cm

$F_{pu} = 3.904\,F_{py}$ (attained at 0.8 D_{TM})

* m_i = mass of floor i. Other terms are defined in Figure 22 or in the text.

Perimeter walls are modelled by a spring and hysteretic damper in-parallel (one set on each side of the building) that contact the 1st-floor slab when its displacement exceeds the moat width. The wall spring is elastic-plastic, and the damper provides a retarding force (opposing the velocity of the 1st floor) whose amplitude is 60% of the spring force (Figure 22, Table 4).

The superstructure exceeds UBC requirements. The code lateral-force coefficient V/W has been taken as 0.156, and the story yield strengths are based on the coefficient $0.156 \cdot (1.7 / 1.33) = 0.20$. Ultimate story strengths are 40% higher. Details of the story force-displacement curves appear in Figure 22 and Table 4. The fundamental period of the elastic fixed-base superstructure is 0.52 seconds. Stiffness-proportional viscous damping is added to the superstructure in the form of dampers parallel to the story shear springs, with damping value in story i equal to $(2\xi'' T_1 / 2\pi) k_i$, where $\xi'' = 0.05$ and $T_1 = 0.52$ sec. The force capacity of a story damper is set to 0.20 of the story shear-spring strength F_{iu}. P-Δ effects are included for the superstructure (but not the pads) for story heights of 381 cm.

Although the base-isolated building's design is intended to be realistic, there are many parameters which can vary over a wide range, and so the results obtained below should be regarded with this in mind. There is also a considerable amount of idealization and uncertainty in the structural and nonlinear modelling. Properties of the perimeter wall are especially uncertain, and more work is needed to quantify behavior of the isolation pads at large displacements. The amount of inelastic action in the building depends on the ultimate strength of the pads, which is not well defined, and on the building's story strengths and damping. These story strengths and damping have been chosen on the high side to reduce the chance that the model would exaggerate the degree of inelastic action. On the other hand, the use of a shear building tends to localize the yielding.

The 3-story base-isolated building is analyzed first for the N-S Sylmar ground motion from the Northridge earthquake. For the 40/0 design, the building strikes its perimeter wall with a velocity of 78 cm/sec. Following the impact, the 1st story displaces laterally to 19 cm, corresponding to a drift of 5.0%. For reference, the elastic-limit drift in the 1st story is 0.2% (for all designs). The effects of moat width (D_{TM}) and added damping (B') are shown in Table 5 (N-S Sylmar motion) where all designs are compared. Although impact still occurs for the 40/5 design, increasing B' to 10% (40/10) is enough to eliminate the impact. The building yields in all the designs; the 1st-story drift varies from 5.0% for 40/0 to 1.1% for 60/10, and it reaches 2.8% in the fixed-base building.

TABLE 5

Summary of responses of base-isolated and fixed-base designs of 3-story building

	1994 N-S Sylmar			Simulated M_W7.0 Ground Motions						
Design	Peak striking velocity	Peak pad disp.	Peak 1st-story drift	Area of impacts	Peak striking velocity C5	Peak pad disp. C5	Peak 1st-story drift C5	Area over which 1st-story drift exceeds		
D_T/B' (cm/%)	(cm/sec)	(cm)	(%)	(km^2)	(cm/sec)	(cm)	(%)	*1%* (km^2)	*3%* (km^2)	*8%* (km^2)
40/0	78	42	5.0	625	138	47	*	625	500	325
40/5	49	41	2.8	475	121	45	*	475	450	225
40/10	0	38	1.0	450	106	44	19.1	450	375	225
50/0	0	45	1.9	350	116	55	*	575	325	225
50/5	0	39	1.7	225	98	53	19.8	500	250	200
50/10	0	35	1.2	175	77	52	14.0	475	225	150
60/0	0	42	2.1	75	70	62	20.7	525	300	175
60/5	0	36	1.6	25	0	57	12.3	475	300	150
60/10	0	32	1.1	0	0	51	10.4	450	250	150
Fixed Base	–	–	2.8	–	–	–	4.9	825	350	25

*Collapse occurs.

For the M_W7.0 ground motion at site C5, lateral displacement time histories of the pads and 1st story are plotted in Figure 23 for two isolated designs (40/0 and 60/10) and the fixed-base building. Impact occurs for the 40/0 design, which is quite severe (striking velocity = 138 cm/sec). In the post-impact response of the 40/0 design, the momentum of the building carries it far into an inelastic excursion during which a P-Δ collapse occurs.

Although the 60/10 design eliminates impact, the drift in the 1st story reaches 10.4%, while that for the fixed-base building is only 4.9%. And even though collapse does not occur for either design, no deterioration mechanisms have been included.

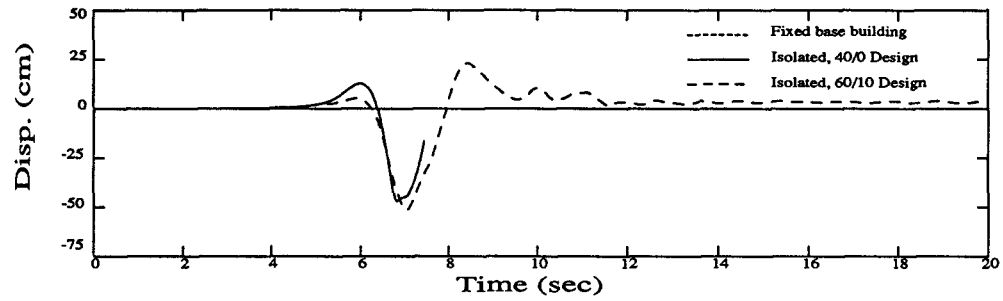

(a) Pad shearing displacenment

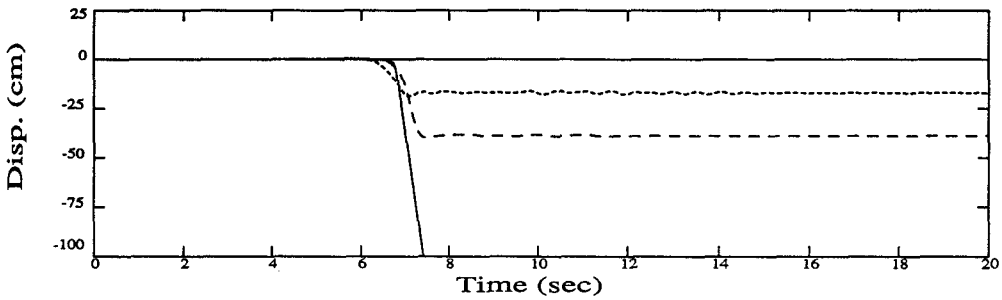

(b) Lateral displacement in 1st story

Figure 23 Lateral displacement time histories of the pads and 1st-story of the 3-story building for the C5 ground motion for three cases: fixed-base building, isolated building with D_T = 40 cm and B' = 0, and isolated building with D_T = 60 cm and B' = 10%.

The calculations for the M_w7.0 earthquake are repeated for every location in the 11 × 11 grid to define the extent of the region over which severe effects occur. Results for the 40/0 design are shown in Table 6 as peak values of pad displacement (>40 cm means impact occurs) and drift in the 1st story. The area of the region over which impact occurs is about 625 km^2 which includes the region where large story drifts are generated. First-story drifts exceed 3% over a region of 500 km^2. Although the building model probably underestimates accelerations associated with the impacts, even at the 2nd floor the model accelerations are about 500 cm/sec^2 within the region of impact.

A comparison of the performance of all the designs for the M_w7.0 earthquake is contained in Table 5. Quantities tabulated include the areas of the regions of impact; peak values of pad displacement, striking velocity and 1st-story drift at site C5; and areas of the regions where peak 1st-story drifts of 1%, 3% and 8% are exceeded. As seen from Table 5, complete

TABLE 6

Peak responses of the 3-story isolated building with D_T = 40 cm and B' = 0 to the M_w7.0 ground motions at the 121 stations: pad displacement and 1st-story drift.

	1	2	3	4	5	6	7	8	9	10	11	
K	8.	8.	17.	18.	14.	7.	5.	3.	4.	4.	3.	
J	7.	11.	20.	37.	41.	17.	10.	7.	5.	5.	3.	
I	9.	20.	30.	43.	47.	35.	10.	9.	4.	5.	3.	
H	12.	19.	32.	42.	45.	42.	29.	9.	5.	4.	4.	Peak
G	9.	21.	28.	43.	46.	41.	40.	3.	4.	3.	3.	pad
F	12.	25.	29.	44.	47.	42.	19.	5.	4.	5.	4.	disp.
E	9.	30.	33.	45.	47.	44.	14.	7.	4.	5.	2.	(cm)
D	14.	28.	33.	45.	49.	42.	14.	5.	5.	5.	3.	
C	12.	21.	28.	44.	47.	42.	22.	8.	5.	4.	3.	
B	11.	14.	19.	41.	44.	41.	21.	11.	6.	4.	3.	
A	8.	8.	12.	30.	39.	36.	36.	17.	10.	3.	2.	

K	0.1	0.1	0.1	0.2	0.1	0.1	0.1	0.1	0.1	0.1	0.1	
J	0.1	0.1	0.2	0.8	3.1	0.2	0.1	0.1	0.1	0.1	0.1	
I	0.1	0.2	0.5	4.8	19.3	0.6	0.1	0.1	0.1	0.1	0.1	Peak
H	0.1	0.2	0.6	4.4	*	1.8	0.4	0.1	0.1	0.1	0.1	1st-story
G	0.1	0.2	0.4	7.0	*	2.3	1.1	0.1	0.1	0.1	0.1	drift
F	0.1	0.3	0.5	8.9	*	3.2	0.2	0.1	0.1	0.1	0.1	(% of
E	0.1	0.4	0.6	17.9	*	8.8	0.1	0.1	0.1	0.1	0.1	story
D	0.1	0.5	0.6	17.7	*	6.6	0.1	0.1	0.1	0.1	0.1	height)
C	0.1	0.2	0.4	8.6	*	4.9	0.2	0.1	0.1	0.1	0.1	
B	0.1	0.1	0.2	1.1	9.9	2.1	0.2	0.1	0.1	0.1	0.1	
A	0.1	0.1	0.1	0.5	0.8	0.7	0.7	0.1	0.1	0.1	0.1	

elimination of the impacts is accomplished only by the 60/10 design. However, this design still transfers considerable force up into the building for near-source locations. For example, 1st-story drifts exceeding 3% occur over a region of 250 km^2 for design 60/10. The fixed-base building has smaller story drifts over a wider area. In terms of 1st-story drift, the advantage of base isolation is only apparent outside the near-source region. For some near-source sites, base isolation as modelled here may actually be a disadvantage. Also, although not considered here, uplift is a concern, especially for taller buildings.

Isolation devices other than the flexible pads considered here, such as sliding and ball-bearing systems, could be better in accommodating the very large displacements at locations close to large earthquakes and should also be further studied. However, difficulties in designing flexible utility connections to take such movements would have to be overcome.

CONCLUSIONS

Generated ground motion in the vicinity of a large earthquake, such as the M_w7.0 thrust event considered here, contains a large, rapid displacement pulse which can produce structural response in tall fixed-based buildings more severe than anticipated by code writers. The forward and back (reversing) displacement pulse can be very effective in causing damage if the duration of the pulse is comparable to the fundamental period of vibration of the structure. Even if weld fracture does not occur, the strongest of the generated ground motions for the M_w7.0 thrust earthquake, perhaps covering a region of about 500 km^2 in the near field, are capable of causing severe distress in the 20-story code-designed building analyzed, with the possibility of collapse at some sites. If the susceptibility of welded connections to fracture is taken into account, then the collapse potential increases markedly. It should also be noted that the 20-story building was only analyzed in its short direction, which would be stronger than in the long direction where wind does not control the design.

A typical isolated building on flexible pads with a moat width of 40 cm, a dimension exceeding that in several existing Southern California isolated buildings, would impact its perimeter wall or other barrier device if located within the near-source region of a moderate to large earthquake. Such impacts cause damage to the structure as well as to its contents, decreasing the likelihood that the facility can remain functional following the earthquake. Eliminating these impacts requires exceptional design measures for the isolation system. For the M_w7.0 thrust earthquake and the 3-story building analyzed, impacts occur over a region of significant extent (about 625 km^2) when a 40-cm moat width is used. Possibility of collapse exists over perhaps half of this area. Increasing the moat width to 60 cm and adding extra pad damping of 10% of critical eliminates the impacts, but excessive yielding in the building still occurs for sites in the near-source region. Larger earthquakes would place even greater demands on the building.

In view of the many assumptions made in the analyses performed here, the above conclusions should be regarded as preliminary, and this is strongly emphasized. This is especially true for the analysis of the 20-story building where more work is needed to include or better account for multidirectional ground motion, foundation behavior, soil-structure interaction, structural degradation including weld fracture, three-dimensional effects, and additional contributors to the lateral resistance. Doing so could either moderate or worsen the structural performance predicted here. Additional building heights and configurations need to be examined. More research should be devoted to effects of large-magnitude earthquakes regarding duration of shaking and long-period content, in addition to near-source effects.

Regarding the issue of whether base isolation is a good idea or not, the results given here provide useful information but do not answer the question. The answer is site dependent and would have to consider the size of the design earthquake, probability of being in a near-source region, desired performance of the structure, type of isolation system employed (including future improvements), and economic considerations.

REFERENCES

J.C. Anderson and V.V. Bertero, 1987. Uncertainties in establishing design earthquakes, *Journal of Structural Engineering*, ASCE, Vol. 113, No. 8, August, pp. 1709-1724.

R. Archuleta and S. Hartzell, 1981. Effects of fault finiteness on near source ground motion, *Bulletin of the Seismological Society of America*, Vol. 71, pp. 939-957.

V.V. Bertero, S.A. Mahin and R.A. Herrera, 1978. Aseismic design implications of near-fault San Fernando earthquake records, *International Journal of Earthquake Engineering and Structural Dynamics*, Vol. 6, No. 1, Jan.-Feb., pp. 31-42.

V.V. Bertero, J.C. Anderson and H. Krawinkler, 1994. Performance of steel building structures during the Northridge earthquake, UCB/EERC 94/09, Earthquake Engineering Research Center, University of California, Berkeley.

B.A. Bolt, 1968. The focus of the 1906 California earthquake, *Bulletin of the Seismological Society of America*, Vol. 58, pp. 457-471.

D.M. Boore, W.B. Joyner and T.E. Fumal, 1993. Estimation of response spectra and peak accelerations from western North American earthquakes: an interim report, U.S. Geological Survey, Open File Report 93-509.

J.N. Brune, 1970. Tectonic stress and spectra of seismic shear waves from earthquakes, *Journal of Geophysical Research*, Vol. 75, pp. 4997-5009.

J.P. Buwalda and P. St. Armand, 1955. Geologic effects of the Arvin-Tehachapi earthquake, earthquakes in Kern County, California during 1952, G. B. Oakeshott, California Division of Mines and Geology, Bulletin 171, 41-56.

V. Murty Challa and J.F. Hall, 1994. Earthquake collapse analysis of steel frames, *Earthquake Engineering and Structural Dynamics*, Vol. 23, No. 11, November, pp. 1199-1218.

R. Darragh, et al., 1994. Processed CSMIP strong-motion records from the Northridge, California earthquake of January 17, 1994: Release No. 1, California Strong Motion Instrumentation Program, Department of Conservation, Division of Mines and Geology, Sacramento, California, February.

J.F. Dolan, K. Sieh, T.K. Rockwell, R.S. Yeats, J. Shaw, J. Suppe, G.J. Huftile and E.M. Gath, 1995. Prospects for larger or more frequent earthquakes in the Los Angeles metropolitan region, *Science*, Vol. 267, January 13, pp. 199-205.

M.D. Engelhardt, and A.S. Husain, 1993. Cyclic-loading performance of welded flange-bolted web connections, *Journal of Structural Engineering*, ASCE, Vol. 119, No. 12, December.

A. Frankel, 1993. Three-dimensional simulations of ground motions in the San Bernardino Valley, California, for hypothetical earthquakes on the San Andreas fault, *Bulletin of the Seismological Society of America*, Vol. 83, pp. 1020-1041.

S.H. Hartzell and T.H. Heaton, 1990. Earthquake ground motion at close distances, *EPRI/Stanford/USGS Workshop*, Palo Alto, California, Sept.

T.H. Heaton, 1990. Evidence for and implications of self-healing pulse of slip in earthquake rupture, *Physics of Earth and Planetary Interiors*, Vol. 64, pp. 1-20.

T.H. Heaton, J.F. Hall, D.J. Wald and M.W. Halling, 1995. Response of high-rise and base-isolated buildings to a hypothetical M_W7.0 blind thrust earthquake, *Science*, Vol. 267, January 13, pp. 206-211.

T.H. Heaton and S.H. Hartzell, 1988. Earthquake Ground Motions, *Annual Reviews of Earth and Planetary Sciences*, Vol. 16, pp. 121-145.

S.E. Hough, 1995. Earthquakes in the Los Angeles metropolitan region: a possible fractal distribution of rupture size, *Science*, Vol. 267, January 13, pp. 211-213.

International Conference of Building Officials, 1991, 1994. *Uniform Building Code*, Whittier, California.

W.D. Iwan and X.D. Chen, 1994. Important near-field ground motion data from the Landers earthquake, *Proceedings of the 10th European Conference on Earthquake Engineering*, Vienna.

A. Olson, J. Orcutt and G. Frazier, 1984. The discrete wavenumber/finite element method for synthetic seismograms, *Geophysical Journal of the Royal Astronomical Society*, Vol. 77, pp. 421-460.

C.F. Richter, 1958. *Elementary Seismology*, W. H. Freeman and Company, Inc., San Francisco.

K.E. Sieh, et al., 1993. Near-field investigations of the Landers earthquake sequence, April to July 1992, *Science*, Vol. 260, 171-176.

Seismology Committee of the Structural Engineers Association of California, 1990. *Recommended Lateral Force Requirements and Commentary*, Sacramento, California.

P.G. Somerville, and R.W. Graves, 1993. Conditions that give rise to unusually large long period ground motions, *Structural Design of Tall Buildings*, Vol. 2, pp. 211-232.

K.-C. Tsai and E.P. Popov, 1988. Steel beam-column joints in seismic moment resisting frames, UCB/EERC 88/19, Earthquake Engineering Research Center, University of California, Berkeley, November.

D.J. Wald and T.H. Heaton, 1994a. Spatial and temporal distribution of slip for the 1992 Landers, California earthquake, *Bulletin of the Seismological Society of America*, Vol. 84, pp. 668-691.

D.J. Wald and T.H. Heaton, 1994b. A dislocation model of the 1994 Northridge earthquake determined from strong ground motions, *U.S. Geological Survey Open File Report 94-278.*

Working Group on California Earthquake Probabilities, 1988. Probabilities of large earthquakes occurring in California on the San Andreas fault, *U.S. Geological Survey Open File Report 88-398.*

Working Group on California Earthquake Probabilities, 1990. Probabilities of large earthquakes in the San Francisco Bay region, California, *U.S. Geological Survey Circular 1053.*

1994 Working Group on the Probabilities of Future Large Earthquakes in Southern California, 1995. Seismic hazards in Southern California: probable earthquakes 1994-2024, *Bulletin of the Seismological Society of America*, Vol. 85, pp. 379-439.